THE JOURNAL OF PHYSICAL CHEMISTRY A

Article

pubs.acs.org/JPCA

Spectroscopic Characterization and Constitutional and Rotational Isomerism of ClC(O)SCN and ClC(O)NCS

Luis A. Ramos,[†] Sonia E. Ulic,[†,‡] Rosana M. Romano,[†] Mauricio F. Erben,[†] Yury V. Vishnevskiy,[§] Christian G. Reuter,[§] Norbert W. Mitzel,[§] Helmut Beckers,[∥] Helge Willner,[∥] Xiaoqing Zeng,[∥] Eduard Bernhardt,[∥] Maofa Ge,[⊥] ShengRui Tong,[⊥] and Carlos O. Della Védova.*[,†]

[†]CEQUINOR (UNLP-CONICET), Departamento de Química, Facultad de Ciencias Exactas, Universidad Nacional de La Plata, 47 esq. 115, 1900 La Plata, República Argentina

[‡]Departamento de Ciencias Básicas, Universidad Nacional de Luján, Rutas 5 y 7 (6700) Luján, Argentina

[§]Universität Bielefeld, Lehrstuhl für Anorganische Chemie und Strukturchemie, Universitätsstraße 25, 33615 Bielefeld, Germany

[∥]Fachbereich C - Anorganische Chemie, Bergische Universität Wuppertal, 42097 Wuppertal, Germany

[⊥]State Key Laboratory for Structural Chemistry of Unstable and Stable Species, Beijing National Laboratory for Molecular Sciences (BNLMS), Institute of Chemistry, Chinese Academy of Sciences, Beijing 100080, Peoples Republic of China

Supporting Information

ABSTRACT: Chlorocarbonylthio- and isothiocyanate (ClC(O)SCN and ClC(O)NCS) have been isolated and characterized by IR (Ar matrix, gas), Raman (liquid), ^{13}C NMR and UV−visible spectroscopies. Vibrational and quantum chemical studies suggest the presence of the *syn* and *anti* conformers (SCN group with respect to the C═O bond) in the gas phase for both constitutional isomers. *syn*-ClC(O)SCN is preferred by ΔH° (*anti/syn*) = 1.3(0.3) kcal mol^{-1}. The solid-state structure of ClC(O)SCN has been determined by single crystal X-ray diffraction analysis at low temperature. The crystalline solid consists exclusively of molecules in the *syn* conformation. On the other hand, the *anti* form is more stable for the ClC(O)NCS isomer. The structure of ClC(O)NCS and its conformational composition were determined by gas electron diffraction. An unusual low *syn* → *anti* interconversion energy barrier of 0.98 (0.15) kcal mol^{-1} was detected for ClC(O)NCS at cryogenic temperatures. The photochemistry of both constitutional isomers isolated in solid argon at 15 K was studied. Rearrangement of ClC(O)SCN to ClC(O)NCS was observed in the neat liquid and under UV−vis irradiation of ClC(O)SCN isolated in solid argon. Properties have been discussed in terms of the valence electronic structure, including the analysis of the He(I) photoelectron spectrum of ClC(O)SCN.

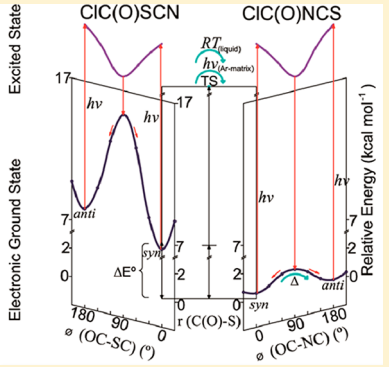

INTRODUCTION

Carbonyl-thiocyanates of the general formula RC(O)SCN have been scarcely studied, probably because of their relative instability.[1−4] Acyl and aryl thiocyanates were detected during the decomposition of 5-(acylthio/arylthio)-1,2,3,4-thiatriazoles (eq 1), and they immediately isomerized to the thermodynamically more stable isothiocyanate isomers, RC(O)NCS.[1] As previously recognized, the rearrangement rates depend on the R group, and usually aryl compounds are more stable than the acyl homologues. Even more, RC(O)SCN compounds seem to be stabilized by resonance effects when they carry aromatic or β-unsaturated substituents R, as well as by the presence of branched substituent groups ($(CH_3)_3C-$, $(Ph)_3C-$). This reveals the influence of steric effects on the isomerization mechanisms.[2]

By using quantum chemical calculations, Koch and Wentrup reported very recently a number of 1,2-, 1,3-, and 1,4-shifts of substituent groups as well as several [3,3]-sigmatropic shifts and retro-ene type reactions of (thio)-cyanates and iso(thio)-cyanates.[5−7]

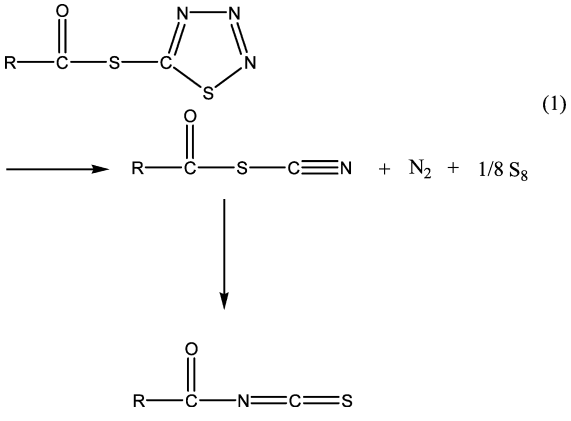

(1)

Received: January 9, 2013
Revised: February 14, 2013
Published: February 17, 2013

The cyanuration of sulfenylcarbonyl compounds, XC(O)SY, represents a suitable method for the preparation of carbonyl thiocyanates (eq 2) such as XC(O)SCN (X = F, Cl)[3] and more recently the methoxy derivate (X = CH_3O).[8] Liquid FC(O)SCN easily isomerizes to FC(O)NCS at room temperature and a bimolecular displacement mechanism S_N2 was proposed considering the strong dependence of the rearrangement rate on solvent and catalytic effects. Interestingly, this rearrangement is reversed by photolysis of FC(O)NCS isolated in an argon matrix at low temperature.[9]

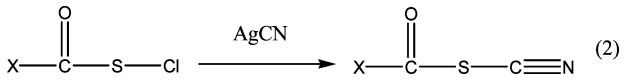

(2)

Both thio- and isothiocyanate isomers adopt planar structures and the preference of the *syn* orientation of the SCN or NCS group with respect to the C═O bond was verified for X = F[9] and CH_3O[8] derivates. A remarkable difference between the rotational energy barrier, E_a, between both stable conformers (*syn*/*anti*) in both constitutional isomers was determined. For FC(O)NCS, the unusual low *anti* → *syn* rotational interconversion barrier observed at cryogenic temperatures (14−18 K) was interpreted in terms of a very low rotational barrier about the C−N bond, which was experimentally determined to be 0.26 ± 0.04 kcal mol^{-1}.[9]

The interesting properties of the XC(O)SCN/XC(O)NCS systems prompted us to characterize the almost unexplored isomers with X = Cl, which are described within this work. A detailed vibrational characterization, together with the study of the conformational properties of both ClC(O)SCN and ClC(O)NCS are presented. Results from IR (gas, Ar matrix), Raman (liquid), ^{13}C NMR, UV−visible spectroscopies, and quantum chemical calculations were undertaken. For the ClC(O)SCN isomer, its X-ray diffraction pattern at low temperature and He(I) photoelectron spectrum was measured, and for the ClC(O)NCS the gas-phase structure was determined by electron diffraction. The constitutional isomerization of ClC(O)SCN to ClC(O)NCS was evaluated by IR spectroscopy. Both isomers were isolated in solid Ar at cryogenic temperatures, and their thermal and photochemical behaviors were evaluated.

RESULTS AND DISCUSSION

General Properties. Both, ClC(O)NCS and ClC(O)SCN, are colorless liquids at room temperature. The isothiocyanate isomer melts at −89 °C[10] and the vapor pressure over the temperature range −54 to 20 °C follows the equation ln p_v [atm] = −4650(42) (1/T[K]) + 12.0(2) (Figure S1 in Supporting Information, uncertainty of the linear fit are quoted in parentheses), which leads an extrapolated boiling point of 115(2) °C. On the other hand, ClC(O)SCN melts at −6 °C, and its vapor pressure at 15 °C is 8 mbar. The vapor pressure curve for the thiocyanate isomer could not be determined because of the high instability of this compound even at room temperature. Both constitutional isomers are air sensitive and immediately react with water. Samples should be handled in vacuum flame-sealed vessels and kept at −196 °C to prevent decomposition. By contrast, both ClC(O)SCN and ClC(O)NCS are stable in the gas phase, even if heated to 100 °C.

The ^{13}C NMR spectrum of ClC(O)SCN shows two singlets with chemical shifts of 158.9 and 105.6 ppm, which are assigned to the carbon atoms of the C(O) and SCN groups, respectively (Figure S2). The ^{13}C NMR spectrum of ClC(O)NCS is in accordance with previous experiments (δ = 140.5 ppm (CO) and δ = 154.2 ppm (NCS)).[10] Both ^{13}C NMR spectra agree well with chemical shifts reported for related compounds.[9] The UV−visible spectra of both gaseous isomers are shown in Figure S3. The spectrum of ClC(O)SCN shows two absorptions, with $\lambda_{max} \approx$ 190 nm and another weak band at 218 nm. These absorptions are assigned, by comparison with related molecules, to the $\pi \rightarrow \pi^*$ and $n_s \rightarrow \pi^*$ transitions within the C═O and SCN groups, respectively. Red-shifted bands are observed for ClC(O)NCS, and the absorptions at $\lambda_{max} \approx$ 197 and 262 nm are also attributed to the $\pi \rightarrow \pi^*$ (CO) and $n_s \rightarrow \pi^*$ (NCS) transitions.[9]

Quantumchemical Calculations. To evaluate the conformational equilibrium of ClC(O)SCN and ClC(O)NCS, the potential energy curves for the internal rotation about the C−X (X = S and N) single bonds for both conformers of each isomer were computed by structure optimization at fixed dihedral angles ϕ(OC−XC) from 0° to 180° in steps of 30°, as is shown in Figure 1. Similar curves were obtained at the MP2/6-311+G(d) and B3LYP/6-311+G(3df) levels of theory, which for both compounds revealed two minima at 0° and 180°, corresponding to the *syn* and *anti* conformations (C_s symmetry), respectively.

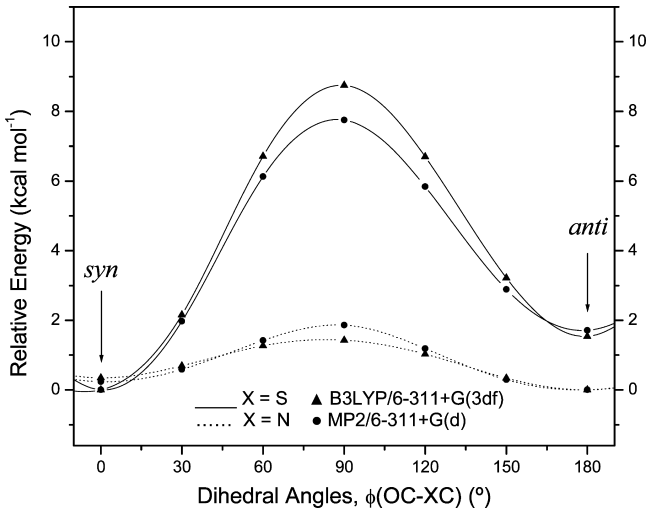

Figure 1. Potential energy curves for the internal rotation around the C−X bonds in ClC(O)SCN (X = S) and ClC(O)NCS (X = N) calculated at the B3LYP/6-311+G(3df) (▲) and the MP2/6-311+G(d) (●) levels of theory.

The molecular structures of *syn* and *anti* ClC(O)SCN and ClC(O)NCS were fully optimized at different levels of approximation, to verify that they correspond to minimum energy structures and to provide zero-point vibrational energy corrections. Computed relative energies for both rotamers are summarized in Table 1. Moreover, optimized structure of the *syn* and *anti* forms of ClC(O)SCN and ClC(O)NCS together with their rotational transition states (TS) are displayed in Figure 2 and their structural parameters are listed in Tables S1 and S2, respectively (in Supporting Information).

For ClC(O)SCN the *syn* form is predicted to be lower in energy ($\Delta E°$) by 1.7/1.4 kcal mol^{-1} with respect to the *anti* rotamer. In contrast, the *anti* form is more stable by 0.3/0.5 kcal mol^{-1} in ClC(O)NCS [MP2/6-311+G(d)]. Similar values, i.e., 1.4 and 0.5 kcal mol^{-1}, respectively, are obtained with the complete basis set CBS-QB3 method. Consequently, a small contribution of roughly 6% is predicted for *anti* form of ClC(O)SCN at room temperature, while a population of 37% is

dx.doi.org/10.1021/jp400281g | J. Phys. Chem. A 2013, 117, 2383−2399

Table 1. Calculated Relative Energies (ΔE^0, including Zero Point Energy Correction, in kcal mol^{-1}), Enthalpies (ΔH^0, kcal mol^{-1}), Gibbs Free Energies (ΔG^0, kcal mol^{-1}) for the *syn* and *anti* Conformers of ClC(O)SCN and ClC(O)NCS and for the Rotational TSs at Different Levels of Theory (at 298.15 K; in kcal mol^{-1})[a]

methods	$\Delta E°$	$\Delta H°$	$\Delta G°$	$\Delta E°$ (TS)	E_a (*anti* → *syn*)
ClC(O)SCN					
B3LYP/6-311+G(d)	1.53	1.52	1.48	7.94	6.41
B3LYP/6-311+G(3df)	1.55	1.52	1.52	8.57	7.02
B3LYP/aug-cc-pVTZ	1.67	1.64	1.64	8.47	6.80
MP2/6-311+G(d)	1.69	1.69	1.59	7.58	5.89
CBS-QB3	1.44	1.44	1.43	8.04	6.60
ClC(O)NCS					E_a (*anti* → *syn*)
B3LYP/6-311+G(d)	0.19	0.19	0.19	1.24	1.05
B3LYP/6-311+G(3df)	0.35	0.36	0.35	1.34	0.99
B3LYP/aug-cc-pVTZ	0.45	0.46	0.43	1.36	0.91
MP2/6-311+G(d)	0.26	0.27	0.30	1.73	1.47
CBS-QB3	0.52	0.52	0.52	1.08	0.57

[a]Energy differences are relative to *syn*-ClC(O)SCN and *anti*-ClC(O)NCS (Figure 2).

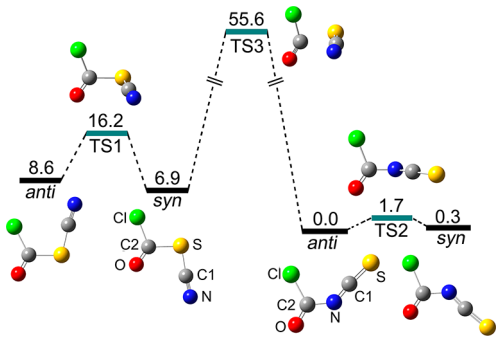

Figure 2. Relative energies (kcal mol^{-1}) of the *syn* and *anti* forms and transition states (TS1, TS2, TS3) of the ClC(O)SCN and ClC(O)NCS molecules calculated at the MP2/6-311+G(d) level of theory.

expected for the *syn* rotamer of ClC(O)NCS according to calculated $\Delta G°$ values (Table 1). The preference of the *syn* form in ClC(O)SCN can probably be explained in terms of the mesomeric (resonance) and anomeric effect.[11] In particular, for this conformer, a major energy stabilization is expected through donation of electron density of the σ-type lone-pair on the sulfur atom into the antibonding orbital of the C═O bond, $lp_\sigma(S) \rightarrow \sigma^*(C{=}O)$, according to the anomeric effect.[12] This feature was also reported for similar molecules such as FC(O)SCN[9] and $CH_3OC(O)SCN$.[8] The electronic properties determined by photoelectron spectroscopy for ClC(O)SCN (see below) support the qualitative picture, which suggests the conformational preference in terms of donor−acceptor interactions. By contrast, the major stability of the *anti* conformer in ClC(O)NCS is intriguing, and calculations suggest that the $lp_\sigma(N) \rightarrow \sigma^*(C{-}Cl)$ delocalization is predominant in the isothiocyanate moiety.

An interesting result that follows from the potential energy curves of both constitutional isomers (Figure 1) is their large difference in rotational barriers. Computed energy barriers E_a for the *anti* → *syn* internal rotation of ClC(O)SCN and *syn* → *anti* for ClC(O)NCS derived from fully optimized transition state structures at various levels of theory are listed in Table 1. The transition state (TS1 and TS2, Figure 2) structures were verified by an intrinsic reaction coordinate (IRC) calculation to connect the conformers along the reaction path for the normal coordinate of the imaginary frequency. Values between 5.9 to 7.0 kcal mol^{-1} were computed for the *anti* → *syn* rotamerization in ClC(O)SCN, whereas very low energy barriers between 0.6 and 1.6 kcal mol^{-1} are predicted for the *syn* → *anti* rotational interconversion of ClC(O)NCS, which agrees with experimental results discussed below.

On the other hand, *anti*-ClC(O)NCS was predicted to be more stable than its constitutional isomer *syn*-ClC(O)SCN by 6.9 kcal mol^{-1} on the MP2/6-311+G(d) level of theory. The transition state (TS3) separating these isomers exhibits C_1 symmetry with the SCN group being perpendicular to the ClC(O) moiety. The calculated energy of TS3 relative to *anti*-ClC(O)NCS amounts to 55.6 kcal mol^{-1} at the same level of theory. This corresponds to an activation energy E_a of 48.7 kcal mol^{-1}, which is lower that the value (53.8 kcal mol^{-1}) recently reported for the related FC(O)SCN/FC(O)NCS system.[9]

Crystal Structure of ClC(O)SCN. By using the low-temperature crystallization, appropriate single crystals of ClC(O)SCN were grown at −20 °C. The compound crystallizes in the orthorhombic space group $P2_12_12_1$ with unit cell dimensions of a = 5.3289(2), b = 5.9150(2), c = 14.2581(6) Å, and Z = 4. Figure 3 shows the molecular structure of ClC(O)SCN in the

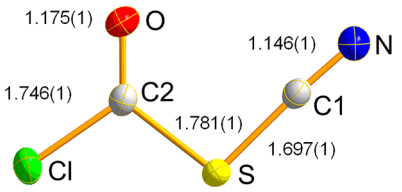

Figure 3. Structure of the ClC(O)SCN molecule in a single crystal at 150 K; thermal ellipsoids are drawn at the 50% probability level.

solid state and Table 2 lists important structural parameters from this experiment, and for comparison, those obtained from quantum chemical calculations, as well as structure parameters reported for related species [ClC(O)SX, X = Cl,[13] CH_3,[13] and CH_2CH_3[14]] in the crystalline phase.

Only the more stable *syn* conformer with nearly planar structure [ϕ(CS−C═O) = 0.3(1)° is observed in the single crystal at 150 K. In general, the main geometric parameters obtained by X-ray diffraction are well reproduced by quantum chemical calculations, i.e., bond lengths and bond angles of the free molecule lie within 0.03 Å and 2° of those obtained in the solid phase. Additionally, the structural parameters obtained by X-ray diffraction of related molecules show values similar to those obtained for the title species, as compared in Table 2.

The dipole moment of ClC(O)SX molecules (X = Cl and CH_3) may contribute to intermolecular interactions in the crystalline state.[13] Recently, the crystal structure refinement of $ClC(O)SCH_2CH_3$, complemented with a topological analysis of the crystal electron density, allowed the characterization of a network of medium-weak to weak intermolecular interactions, with a dominant C−H···O hydrogen bond and a Cl···Cl interaction playing also a relevant role.[14] On the other hand, the crystal packing of FC(O)SCN is dominated by intermolecular interactions between the polar carbonyl and thiocyanate groups.[9] Figure S4 shows the most important nonbonded interactions found for ClC(O)SCN. The molecules interact

dx.doi.org/10.1021/jp400281g | J. Phys. Chem. A 2013, 117, 2383−2399

Table 2. Experimental (X-ray Diffraction) and Calculated Geometric Parameters (Å and Degrees) for the *syn* Conformer of ClC(O)SCN[a]

parameter	ClC(O)SCN[b]	B3LYP/6-311+G(3df)	MP2/6-311+G*	CCSD(T)/cc-pVTZ	$ClC(O)SCH_3$[13]	$ClC(O)SCH_2CH_3$[14]	ClC(O)SCl[13]	FC(O)SCN[9]
r(C−Cl)	1.7464(10)	1.772	1.756	1.760	1.786(2)	1.783(1)	1.775(7)	
r(C1−S)	1.6967(11)	1.692	1.697	1.702	1.723(2)	1.733(1)		1.708(4)
r(C═O)	1.1752(13)	1.174	1.188	1.180	1.172(2)	1.181(1)	1.166(8)	1.177(4)
r(C2−S)	1.7814(11)	1.801	1.797	1.795	1.798(2)	1.783(1)	1.740(7)	1.795(3)
r(C≡N)	1.1462(14)	1.154	1.180	1.163				1.136(4)
∠(Cl−C−S)	107.43(5)	107.4	108.9	107.7	110.0(1)	109.73(5)	105.7(4)	
∠(Cl−C═O)	124.30(8)	124.5	124.4	124.8	120.7(2)	120.95(9)	123.5	
∠(O═C−S)	128.27(9)	128.1	126.7	127.5	129.3(2)	129.33(9)	130.8(6)	129.5(3)
∠(C−S−C)	97.49(5)	99.7	97.3	97.9	99.6(1)	99.62(5)	101.0(2)	94.9(2)
∠(S−C−N)	176.38(10)	175.7	177.2	176.4				177.4(3)
ϕ(O−C−S-C)	0.3(1)	0.0	0.0	0.0		−0.8(1)		0.0

[a]Reported values for crystalline structures of the related ClC(O)SX (X = CH_3, CH_2CH_3, and Cl) and FC(O)SCN species are also given. [b]This work; for atom labeling, see Figure 3.

through two S···N short contacts forming chains arranged in planar sheets. These nonbonded interactions amounts, 3.08 Å (symmetry code: 2−*x*,1/2+*y*,1/2−*z*) and 3.26 Å (symmetry code: *x*,1+*y*,*z*), correspond to shorter values than the sum of the van der Waals radii for sulfur and nitrogen (3.35 Å).[15] The sheets are coupled together via N···C (symmetry code: 1−*x*,−1/2+*y*,1/2−*z*) nonbonded interactions (3.23 Å), mainly dominated by electrostatic interactions. As indicated by the reasonable agreement between the calculated and the experimental solid state molecular parameters, these weak interactions do not distort the molecular geometry significantly.

Gas Phase Structure of ClC(O)NCS. The structure of free molecules of ClC(O)NCS was determined by means of gas electron diffraction (GED). In order to explore the presence of more than one conformer in the vapor phase, three models were tested in the refinement of the GED data: (i) only *syn* conformer, (ii) only *anti* conformer, and (iii) mixture of *syn* and *anti* conformers. Model (i) is at odds with the experimental data, as is shown in the radial distribution difference curve for this model (see Figure 4). Model (ii), with pure *anti* conformer, fits the experimental radial distribution curve much better but still has discrepancies in the region for interatomic distances *r* > 4 Å. The best agreement was obtained assuming a conformational mixture of 84(6) % *syn* and 16(6) % *anti* (iii). Clearly, the shoulder at *r* ≈ 5.3 Å in the radial distribution curve can be attributed solely to the *syn* conformer, which indicates the presence of the higher-energy conformer in the gas phase.

It should be noted that ClC(O)NCS produced very weak diffraction patters with a low signal-to-noise ratio. Therefore the structural *R*-factor for the best model (iii) was relatively large (9.5%) in this study. The disagreement of the model with experimental scattering data is, however, mostly due to random errors (see Figure S6) and should therefore not lead to large systematic errors. This is also supported by the good agreement between model and experimental radial distribution curves (Figure 4), where the high-frequency random errors appear only in the area *r* > 5.5 Å, which has no structural meaning in the case of ClC(O)NCS. The largest correlations between refining parameters in the least-squares refinement (≥0.7) were ∠(Cl−C−N)/∠(Cl−C−O) = −0.92 and ∠(C−N═C)/∠(Cl−C−O) = 0.70. Table 3 lists experimental and quantumchemical structural parameters for ClC(O)NCS.

The C═O bond length in the majority conformer of ClC(O)NCS (*anti*) of 1.183(4) Å compares well with the C═O

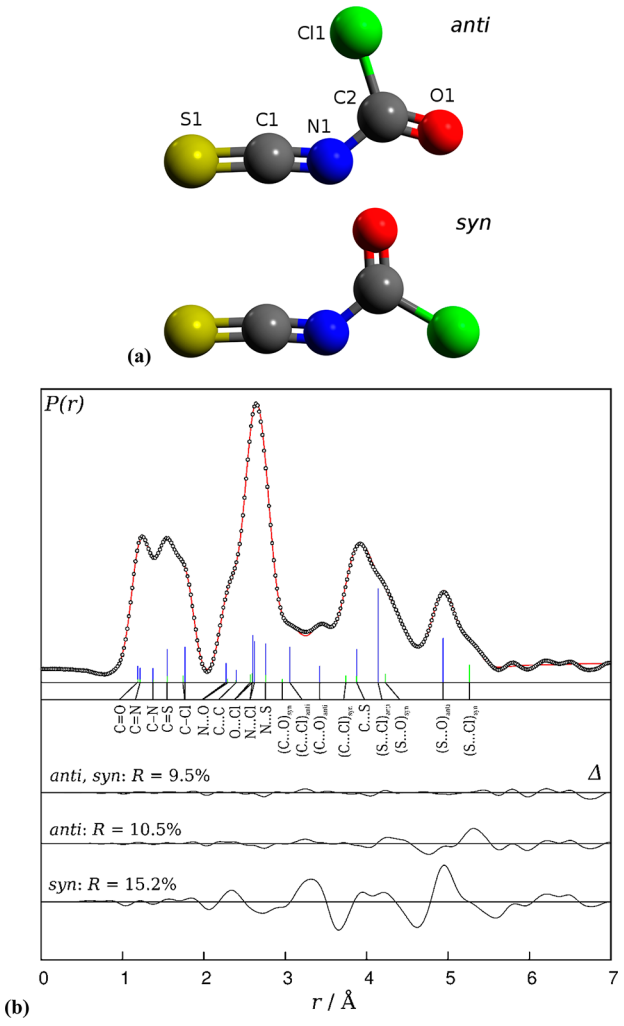

Figure 4. (a) Structures of the two conformers of ClC(O)NCS as determined by GED. (b) Experimental (open circles) and model (line) radial distribution functions. The difference curves for different models are shown below.

distance in phosgene, $OCCl_2$, determined by a joint microwave spectroscopy/quantum chemical approach:[16,17] r_e = 1.1761(13) Å. The C−Cl distance in *anti*-ClC(O)NCS of 1.762(3) Å is slightly longer than the corresponding length in phosgene at 1.7369(6) Å.

dx.doi.org/10.1021/jp400281g | J. Phys. Chem. A 2013, 117, 2383−2399

Table 3. Experimental (GED) and Calculated Molecular Parameters of ClC(O)NCS

	GED				CCSD(T)/cc-pVTZ	
	anti		*syn*		*anti*	*syn*
parameters[a]	r_e, $\angle_e$	r_g	r_e, $\angle_e$	r_g	r_e, $\angle_e$	r_e, $\angle_e$
r(C2−Cl)	1.762(3)[1]	1.769(3)	1.738(3)[1]	1.747(3)	1.771	1.748
r(C2−N)	1.366(4)[2]	1.375(4)	1.370(4)[2]	1.379(4)	1.383	1.387
r(C=O)	1.183(4)[3]	1.187(4)	1.187(4)[3]	1.191(4)	1.185	1.189
r(C1=N)	1.213(4)[4]	1.217(4)	1.212(4)[4]	1.216(4)	1.215	1.216
r(C=S)	1.543(2)[5]	1.549(2)	1.545(2)[5]	1.551(2)	1.558	1.558
∠(Cl−C−N)	112.7(9)[6]		110.4(9)[6]		113.1	110.5
∠(Cl−C=O)	122.3(10)[7]		123.2(10)[7]		122.2	123.1
∠(N−C=O)	125.1(13)[b]		126.4(13)[b]		124.8	126.4
∠(C−N=C)	135.7(12)[8]		135.0(12)[8]		135.8	133.3
∠(N=C=S)	177.2(24)[9]		176.7(24)[9]		175.0	174.6
φ(O=C−N=C)	180.0[c]		0.0[c]		180.0	0.0
x[d], %	84(6)		16(6)		77	23

[a]Vibrational corrections to the equilibrium structure have been calculated using MP2(full)/cc-pVTZ harmonic and cubic force fields. Three times standard deviations are given in parentheses. Superscript numbers 1, 2, ..., 9 represent groups in which parameters were tied together in least-squares method by fixing differences between their values. The constraints were taken from MP2(full)/cc-pVTZ calculations. [b]Dependent parameter. [c]Fixed parameter. [d]Conformational composition. Theoretical values are calculated for 276K using ΔG^0 values.

The O−C−Cl angle in *anti*-ClC(O)NCS at 122.3(10)° is also similar to that in phosgene at 124.07(3)°.

The geometry of the isothiocyanate group can be compared to that in HNCS (structure type r_s, *trans* form)[18] and (C_2H_5)NCS (structure type r_{av}, *cis* form),[19] for which gas phase structures have been reported. The bond between the carbonyl C atom and the nitrogen atom in ClC(O)NCS is 1.366(4) Å and thus much shorter than the corresponding bond between the NCS group and the alkyl C atom in (C_2H_5)NCS at 1.520(8), which corresponds to a C−N single bond. This leads to the conclusion that the ClC(O)−NCS bond has partial multiple bond character.

The C−N bond within the NCS group in ClC(O)NCS has a length of 1.213(4) Å, and is thus more similar to the corresponding bond in HNCS [1.207(7) Å (3σ)] and longer than that in (C_2H_5)NCS [1.187(15) Å (3σ)]. The C−S bond in ClC(O)NCS has a length of 1.543(2) Å and is therefore slightly shorter than in HNCS at 1.567(2) Å and more substantially shorter than in (C_2H_5)NCS 1.580(12) Å. In contrast, the values for the N−C−S angles are similar 177.2(24)° for ClC(O)NCS, 173.8(69)° for HNCS and 173.5(90)° for (C_2H_5)NCS.

Electron diffraction patterns were also measured for ClC(O)-SCN. However, all our attempts to refine the structure and the conformational composition of this compound failed. The obtained data could not be described satisfactorily by models of this compound. This is probably due to the fact that this compound is rather unstable and decomposed under the experimentally applied conditions. The decomposition route of ClC(O)SCN will be discussed below.

Vibrational Spectra. The Ar-matrix IR, gas-phase IR, and liquid-state Raman spectra were recorded for ClC(O)SCN, and they are shown in Figure 5. The experimental frequencies together with those obtained from B3LYP/6-311+G(3df) calculations and their tentative assignments are listed in Table 4. As mentioned before, theoretical calculations predict a *syn/anti* conformational equilibrium for ClC(O)SCN in the gas phase at room temperature. The gas phase and Ar-matrix IR spectra agree with the presence of a small contribution of the higher energy conformer (*anti*). For each conformer, $3N - 6 = 12$ normal modes of vibrations are expected, which can be divided in $2N - 3 = 9$ modes of symmetry A′ and $N - 3 = 3$ modes of symmetry A″ in the C_s point group of symmetry.

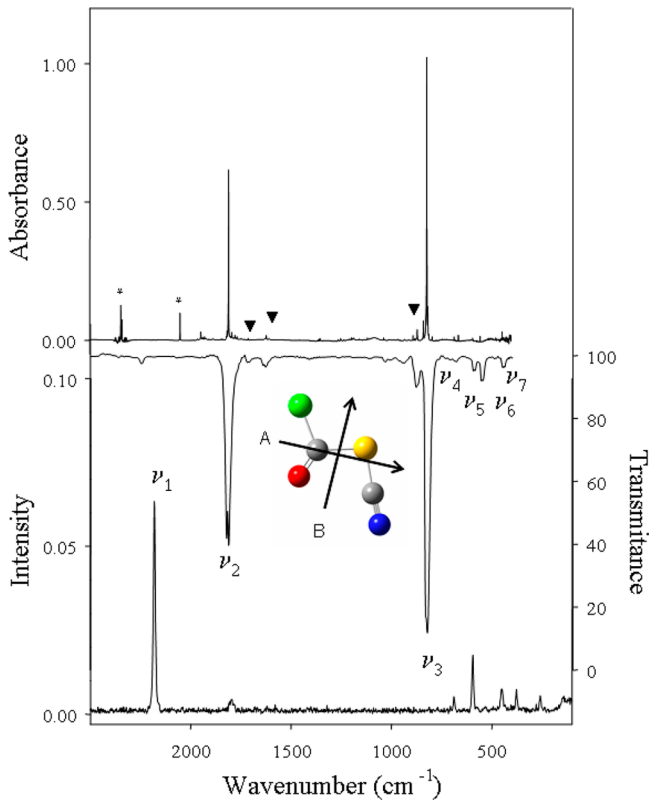

Figure 5. Upper trace: IR spectrum of ClC(O)SCN isolated in an Ar matrix at 15 K (resolution: 0.25 cm^{-1}). Middle trace: IR spectrum of gaseous ClC(O)SCN at 298 K (resolution: 2 cm^{-1}). Lower trace: Raman spectrum of liquid ClC(O)SCN at 298 K (resolution: 2 cm^{-1}). Molecular structure and the principal axes of inertia of *syn* ClC(O)SCN are shown in the inset. The C axis is perpendicular to the AB plane. *Impurity bands. ▼ bands of anti ClC(O)SCN.

The characteristic C≡N stretching mode is assigned to the most intense signal of the liquid-state Raman spectrum observed at 2182 cm^{-1}, which is observed as a low absorption at 2220 cm^{-1} in the IR spectra. This mode appears close to the values reported for the molecules FC(O)SCN (2187 cm^{-1})[9] and $CH_3OC(O)SCN$

dx.doi.org/10.1021/jp400281g | J. Phys. Chem. A 2013, 117, 2383−2399

Table 4. Experimental and Calculated Frequencies (cm^{-1}) and Assignment of Vibrational Modes of ClC(O)SCN

	exp.				calc.[c]		
	IR		Raman				
mode	gas[a]	Ar matrix[b]	liquid[b]	solid	*syn*	*anti*	assignment[d]/symmetry
ν_1	2220 (vw)		2182 (100)	2183	2279 (3)	2272 (4)	ν(C≡N)/A′
ν_2	1819 (s), (B), ΔPQ-QR=10	1807.7 (43)	1796 (5)	1778	1865 (265)		ν(C═O)/A′
	1780 (vw)	1776.4 (0.5)				1829 (377)	
		1765.9 (0.3)					
	1716 (vw)	1710.4 (0.3)					
	1633 (vw)	1620.0 (0.9)					$2\nu_3$
	1033 (vw)	1035.3 (0.3)					
	940 (vw)						
		889.1 (0.9)					
		880.2 (0.3)					
ν_3	878 (w)	868.1 (3.6)				853 (326)	ν_{as}(ClCS)/A′
	819 (vs) (A), ΔPR=9	820.8 (100.0)			801 (452)		
		815.0 (12.2)					
ν_4	680 (vw)	684.2 (0.4)	687 (6)	692	700 (4)	707 (13)	ν(S−C(N))/A′
ν_5	590 (vw)	591.8 (0.5)	594 (26)	598	589 (2)	565 (3)	ν_s(ClCS)/A′
ν_6	556 (vw)	554.4 (0.7)			560 (3)	522 (10)	γ(CO), τ(OCSC)/A″
ν_7	443 (vw)	444.4 (1.0)	449 (10)	453	443 (13)	452 (17)	ν(C−Cl), δ(ClCO)/A′
ν_8					404 (2)	402 (2)	oop(CN)/A″
ν_9			377 (9)	384	373 (0)	393 (0)	δ(SCN), ν(C(O)−S)/A′
ν_{10}			257 (7)	261	254 (1)	279 (2)	δ(ClCS)/A′
ν_{11}			141 (6)	139	120 (3)	128 (5)	δ(CSC), δ(SCN)/A′
ν_{12}					76 (2)	68 (5)	τ(OCSC), oop(CN)/A″

[a]Band intensities: vs, very strong; s, strong; w, weak; vw, very weak. Band-type contours are denoted in parentheses. Separation of the wings are denoted by ΔPQ-QR and ΔPR (cm^{-1}). [b]Relative intensities in parentheses. [c]B3LYP/6-311+G(3df) calculated IR frequencies (cm^{-1}) and intensities (km mol^{-1}) in parentheses. [d]ν, δ, τ, and oop represent stretching, deformation, torsion and out of plane modes.

(2178 cm^{-1}).[8] The intense band observed in the IR spectra at 1819 cm^{-1} is assigned to the C═O stretching mode. Considering that the transition dipole moment of the C═O oscillator is almost parallel to the intermediate principal axis of inertia (Figure 5), its B-type contour represents a clear experimental evidence for predominance of the *syn* conformation.[20] Even more, the calculated red-shift ($\Delta\nu$) for the ν(C═O) mode of the *anti* conformer (36 cm^{-1}; B3LYP/6-311+G(3df)) accounts for the presence of a very weak band at 1780 cm^{-1} in the gas phase IR spectrum, which is consequently assigned to the ν(C═O) of the *anti* form. On the other hand, the strongest absorption at 819 cm^{-1} in the IR spectra (gas) is assigned to the Cl−C−S antisymmetric stretching mode (ν_{as}(Cl−C−S)) in comparison with IR spectra of related molecules such as ClC(O)SCl (818 cm^{-1}). The blue-shifted weak band observed at 878 cm^{-1} in the same spectra is attributed to the ν_{as}(Cl−C−S) of the *anti* conformer. The calculated wavenumber shift $\Delta\nu$ of 59 cm^{-1} for this mode is in close agreement with the experimental one (52 cm^{-1}) and supports the assignment. On the other hand, the Cl−C−S symmetric stretching mode (ν_s(Cl−C−S)) is assigned to the intense absorption at 594 cm^{-1} observed in the Raman spectrum of the liquid, in agreement with the calculated frequency (589 cm^{-1}) and previously reported modes for ClC(O)SCl (592 cm^{-1}),[21] ClC(O)SBr (584 cm^{-1}),[22,23] and ClC(O)SCH_2CH_3 (578 cm^{-1}).[24]

The absorption observed at 680 cm^{-1} in the IR (gas) (with a counterpart at 687 cm^{-1} in the Raman spectrum of the liquid) is attributed to the S−C(N) vibration in close agreement with the reported mode for FC(O)SCN (697 cm^{-1}) and $CH_3OC(O)$-SCN (697 cm^{-1}). Moreover, the weak band observed at 556 cm^{-1} in the gas-phase IR spectra is assigned to the out-of-plane deformation (γCO), with a clear C-type band shape expected for A″ modes. This mode represents a further experimental evidence of planarity for the *syn*-ClC(O)SCN conformer.

The vibrational spectrum of ClC(O)NCS was previously described.[25] In Figure 6 the infrared spectrum of matrix isolated ClC(O)NCS in solid Ar is also given and vibrational data are summarized in Table 5.

The gas phase and Ar-isolated IR spectra of ClC(O)NCS are consistent with the calculated *anti*/*syn* conformational equilibrium in the gas phase. The IR spectrum is characterized mainly by the ν_{as}(NCS), ν(C═O), ν(C−N) and ν_{as}(ClCN) vibrational modes as was reported previously.[25] Additionally, weak bands at 1633 cm^{-1} (ClC(O)SCN) and 1725 cm^{-1} (ClC(O)NCS) are observed in the IR spectrum of both constitutional isomers. These bands are attributed to the first overtone of the antisymmetric stretching mode of the ClC(O)X (X = S, N) group. Their intensities are expected to be enhanced through a plausible Fermi resonance with the C═O fundamental absorption. It was also observed for the precursor molecule, ClC(O)SCl, at 1621 cm^{-1}.[21] Even more, for ClC(O)NCS, a weak band at 1667 cm^{-1} in the gas-phase IR spectrum is also observed. This vibrational mode was previously attributed to a combination mode.[25] However, we now reassign this absorption to the first overtone of the ν_{as}(ClCN) stretching mode of the second stable rotamer, the *syn*-ClC(O)NCS.

Matrix Isolation Experiments. The *syn*/*anti* conformational equilibrium of ClC(O)SCN in the gas phase, predicted by quantum chemical calculations (94:6 at B3LYP/6-311+G(3df)), is consistent with IR spectra recorded in the gas phase and in solid Ar (Figure 5). However, more experimental information is desirable to characterize the conformational properties of this compound. The matrix isolation technique can be used to estimate the enthalpy energy difference, ΔH°_{exp}, between stable conformers from IR spectra of mixtures deposited at different nozzle temperatures, provided that the rotational barrier between

dx.doi.org/10.1021/jp400281g | J. Phys. Chem. A 2013, 117, 2383−2399

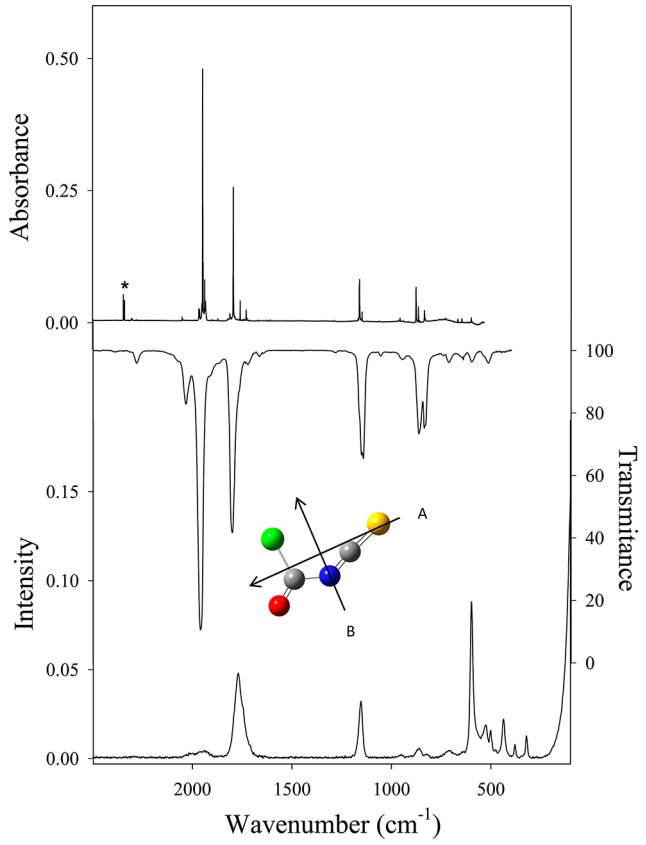

Figure 6. Upper trace: IR spectrum of ClC(O)NCS isolated in an Ar matrix at 15 K (resolution: 0.25 cm^{-1}). Middle trace: IR spectrum of gaseous ClC(O)NCS at 298 K (resolution: 2 cm^{-1}). Lower trace: Raman spectrum of liquid ClC(O)SCN at 298 K (resolution: 2 cm^{-1}). Molecular structure and the principal axes of inertia of the *anti* ClC(O)NCS are shown in the inset. The C axis is perpendicular to the AB plane. *Impurity bands.

the rotamers (*anti* → *syn*) is higher than ≈3 kcal mol^{-1}, which prevents a disturbance of the gas-phase equilibrium composition during the deposition at about 15 K.[26,27] Calculated values for the rotational energy barrier for the *anti* → *syn* interconversion of ClC(O)SCN are shown in Table 1 and are about 7 kcal mol^{-1}.

The two pairs of well-resolved bands observed at 1807.7/1776.4 cm^{-1} (ν_2) and 868.1/820.8 cm^{-1} (ν_3) in the Ar-matrix IR spectrum are assigned to the different rotamers. Temperature-dependent IR spectra reveal an increase in relative intensity of the 1776.4 and 868.1 cm^{-1} absorptions with increasing the nozzle temperatures. They are attributed to the higher energy *anti* conformer. Moreover, the temperature dependence of the integrated intensity ratio (K′) for the two pairs of bands, measured in the temperature range 25−210 °C, was used in a van't Hoff plot (Figure 7). The van't Hoff plot gives an experimental mean value for the *syn* ↔ *anti* conformational equilibrium of ΔH_{exp} = 1.3 (0.3) kcal mol^{-1}, which within the error limits agrees closely well with those obtained at different levels of calculation (Table 1).

On the other hand, attempts to estimate ΔH_{exp} for the constitutional isomer ClC(O)NCS failed because the *syn* → *anti* rotational energy barrier is very low (≈ 1 kcal mol^{-1}; Table 1). However, temperature-dependent Ar-matrix IR spectra were found to be useful to assign vibrational absorptions for both rotamers. Ar-matrix IR spectra of ClC(O)NCS obtained for two different nozzle temperatures at 25 and 200 °C are shown in Figure 8. They exhibit three absorptions instead of the two expected for each vibrational mode due to the *syn*/*anti* conformational equilibrium observed in the gas phase (see Figure 6 and Table 4). At the higher nozzle temperature, the IR intensities of the bands at 1931.9, 1757.4, 1158.8, 830.7, and 722.2 cm^{-1} increase at the expense of the corresponding bands of the anti ClC(O)NCS, and they are assigned to stretching modes of the higher energy *syn* conformer (Table 5). The bands of the most stable form (*anti*) split due to two different matrix environments (S1 and S2; Figure 8).

The small rotational barrier of ClC(O)NCS was evaluated by annealing experiments, as was reported recently for the fluorinated derivative FC(O)NCS, which also exhibits a remarkable very low rotational barrier around the C−N single bond.[9] The Ar-matrix IR spectra of ClC(O)NCS before and after annealing the matrix to 35 K are shown in the Figure 9. Interestingly, the bands assigned to the higher energy *syn* conformer disappear almost completely during the annealing process, which is consistent with the computed small energy barrier for the *syn* → *anti* interconversion. In addition, the intensity of the bands attributed to the *anti* form in the S1 and S2 matrix sites behaved differently, which allowed us to distinguish them (see Table 5). Even more, this result suggests that the *syn* → *anti* interconversion preferentially forms *anti*-ClC(O)NCS isolated in the S2 matrix environment, and consequently, the rotational isomerism depends strongly on the local matrix cage. A similar behavior was also observed in the *cis* → *trans* interconversion of formic acid isolated in solid rare gases, where it was demonstrated that different solid hosts and the local environment can influence strongly the conversion rate constants, although, in this case the mechanism was attributed to a tunneling process.[28]

Our experiments suggest that the conformational equilibrium between *syn*- and *anti*-ClC(O)NCS is particularly interesting for kinetic studies under matrix isolation conditions. Solid argon is known to be rigid enough to prevent diffusion and aggregation of molecules at temperatures around 30 K and consequently a suitable "solid host" for kinetic experiments.[29] For this purpose, time-dependent Ar-matrix IR spectra of ClC(O)NCS were recorded at several temperatures. The conversion of the higher energy *syn* conformer into the *anti* form becomes apparent at temperatures of around 22 K and was followed by monitoring the change of their respective C═O absorptions. The kinetic results are summarized in Table 6. The rate constants, k, were obtained from the first-order decay of the integrated absorption I of the *syn* conformer according to the equation $\ln(I_t/I_0) = -k(t)$. The energy barrier, E_a, for the *syn* → *anti* isomerization, calculated using the Arrhenius equation $\log k = -E_a/2.303RT + \log A$ (A = Arrhenius preexponential factor), yields E_a = 0.98 (0.15) kcal mol^{-1} in the temperature range of 22−31 K (Figure S5 of Supporting Information), which within the uncertainty agrees well with calculated rotational barriers listed in Table 1.

Photochemistry. According to the UV−visible spectra of the constitutional isomers (Figure S3), the use of radiation from a high-pressure mercury lamp should be appropriate for photolysis experiments. The Ar-matrix IR spectra of ClC(O)SCN and ClC(O)NCS before and after photolysis are shown in Figures 10 and 11, respectively.

After 30 min of photolysis using broad band radiation (200 < λ < 800 nm), the intensity of the absorptions of ClC(O)SCN was depleted by about 75% and new bands appeared, which are summarized in Table 7. The strongest new absorption at 2137.9 cm^{-1} is coincident with the ν(CO) mode reported for carbon monoxide.[30]

dx.doi.org/10.1021/jp400281g | J. Phys. Chem. A 2013, 117, 2383−2399

Table 5. Experimental and Calculated Frequencies (cm^{-1}) and Assignment of the Fundamental Vibrational Modes of ClC(O)NCS

Mode	Exp.					Calc.[e]		Assignment[e,f] / Symmetry
	gas[a,b]	gas[c]	Ar matrix[d]		N_2 matrix[d]	*syn*	*anti*	
	2826 vw		2816.8	(<1)	2817.8			
	2560 vw		2540.7	(1.3)	2551.6			
	2285 vw		2302.7	(1.9)	2302.7			$2\nu_3$
	2037 w		1965.0 1961.4	(11.7)				$\nu_3 + \nu_4$
			1946.3 * S1	(100)			2047 (1581)	
ν_1	1963 vs	1963	1936.3 S2		1950.6*			ν_{as}(NCS) / A'
			1931.9	(23.9)		2032 (1846)		
	1804 s	1808	1793.1 S2	(56)	1791.1		1848 (809)	
ν_2			1791.9 * S1					ν(C=O) / A'
	1769 sh	1774	1757.4	(4.9)	1760.9	1812 (397)		
	1725 vw		1726.8 ^{35}Cl	(4.0)	1726.5			$2\nu_4$
	1667 vw		1665.2 ^{37}Cl	(<1)	1667.5			
	1163 sh	1160	1158.8	(7.3)	1158.0	1199 (398)		
ν_3			1156.8 * S1					ν(C–N), ν_s(NCS) / A'
	1150 m	1147	1144.2 S2	(15.4)	1156.9*		1188 (190)	
	947 vw		953.3	(1.4)	953.1			
	862 m	865	872.9 ^{35}Cl 871.4 ^{37}Cl *S2 861.2 ^{35}Cl S1 859.5 ^{37}Cl	(24.2)	868.3*		863 (357)	
ν_4								ν_{as}(ClCN) / A'
	835 m	834	830.7 ^{35}Cl 829.6 ^{37}Cl	(8.1)	830.9 ^{35}Cl 829.7 ^{37}Cl	830 (580)		
	714 w	715	722.2	(<1)		713 (111)		
ν_5			594.8 ^{35}Cl		599.8			ν_s(ClCN) / A'
	599 w	-	592.6 ^{37}Cl	(2.2)	596.1		575 (42)	
	516 w	516					526 (39)	
ν_6		502				500 (4)		δ(NCS) / A'
		439				454 (4)		δ(NCS), ν(ClC) / A'
ν_7		402					428 (8)	ν(ClC), δ(ClCO) / A'
		379					378 (3)	
ν_8		321				310 (<1)		δ(ClCO) / A'
ν_9						80 (<1)	70 (1)	δ(CNC) / A'
ν_{10}	643 w, C	644	642.5	(1.4)	644.0	653 (12)	651 (13)	*oop*(ClCO) / A''
ν_{11}		471				488 (<1)	486 (<1)	*oop*(NCS) / A''
ν_{12}						60 (<1)	69 (1)	τ(OCSC) / A''

[a]This work. [b]Band intensities: vvs, very very strong; vs, very strong; s, strong; m, medium strong; w, weak; vw, very week; sh, shoulder. [c]References 11 and 12. [d]Most intense matrix site, relative intensities are given in parentheses. [e]B3LYP/6-311+G(3df) calculated IR frequencies (cm^{-1}) and intensities (km mol^{-1}) in parentheses. [f]ν, δ, τ, and oop represent stretching, deformation, torsion and out of plane modes, respectively.

Weak bands at 677.4 and 530.7 cm^{-1} are assigned to the S−C and Cl−S stretching modes of ClSCN compared to the reported vibrational data in the gas phase (678.9 and 533.6 cm^{-1}).[31,32] ClSCN is more stable than its isomer ClNCS by about 50 kJ mol^{-1},[31] and it is formed as a byproduct of the CO extrusion.

The new bands located at 1936.3, 1793.3, 1144.4, and 872.5 cm^{-1} in the IR spectra of the photolysis products of ClC(O)SCN can be assigned to the thermodynamically more stable *anti*-ClC(O)NCS isolated in solid argon. Interestingly, the photolytic generated *anti* conformer is mainly detected in the S2 matrix site. Some weak bands

dx.doi.org/10.1021/jp400281g | J. Phys. Chem. A 2013, 117, 2383−2399

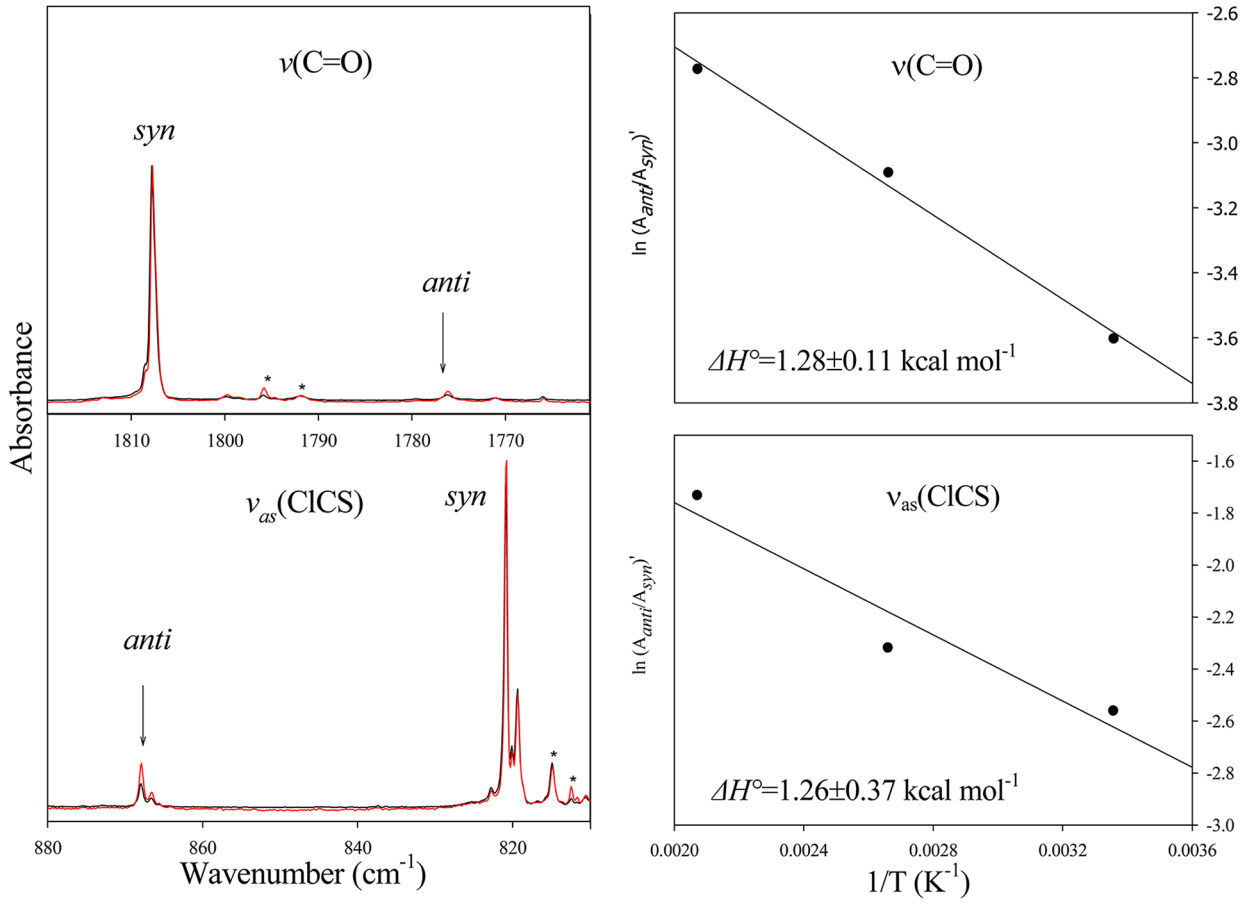

Figure 7. Left traces: IR spectra in the regions of the C═O and Cl−C−S stretching modes of an equilibrium mixture of *syn* and *anti* ClC(O)SCN obtained at nozzle temperatures of 25 °C (black line) and at 210 °C (red line) and deposited in solid argon at 15 K. Intensities are normalized to the ν(C═O) of *syn* ClC(O)SCN. Right traces: van't Hoff plots obtained for the *syn* → *anti* interconversion of ClC(O)SCN. *Impurity bands.

prove the formation of traces of the higher energy *syn*-ClC(O)NCS conformer (Table 7).

When *anti*-ClC(O)NCS isolated in argon was exposed to UV−visible radiation (13 min), a depletion of around 70% of their absorptions was observed in an even faster process than that observed for the ClC(O)SCN species. The matrix was annealed to 35 K before the photolysis until an almost complete *syn* → *anti* rearrangement was reached. The reversed *anti* → *syn* interconversion was observed upon exposure of the deposit to broad band radiation ($200 < \lambda < 800$ nm) as is shown in Figure 11 (upper trace). All absorption bands of the *syn* conformer simultaneously increased at the expense of the bands of the *anti* form. The photoequilibrium is reached by excitation of both rotamers to a level above the internal rotation barrier. The generation of CO and ClSCN was also detected (Table 8). The wavenumber shift from the reported absorption of CO isolated in solid argon[30] is attributed to interactions with ClSCN trapped in the same matrix cage and attributed to a weak band observed at 676.6 cm^{-1}.[32]

The photolytic decomposition channels observed for both constitutional isomers using UV−visible radiation are shown in Figure 12. Main decomposition channel for both isomers is CO extrusion along with the formation of ClSCN molecule. This photodecomposition channel was also observed for the similar molecules FC(O)SCN and FC(O)NCS.[9] However, the ClC(O)SCN → ClC(O)NCS photochemical isomerization detected in this work was not observed for the fluorinated system, where the reversed FC(O)NCS → FC(O)SCN isomerization was observed by photolysis with monochromatic radiation of 193 nm.

Constitutional Isomerism. The isomerization of liquid FC(O)SCN and $CH_3OC(O)SCN$ to the corresponding isothiocyanates has been reported;[3,8] however, no information is yet available for similar processes on the ClC(O)SCN species. ClC(O)SCN was found to be unstable in the liquid state at room temperature − even when stored in vacuum in flame-sealed ampules. Its decomposition becomes evident in a few minutes by the formation of an orange solid, possibly due to the formation of $(SCN)_x$ polymers.[4] To detect the main decomposition products, ClC(O)SCN was distilled into a small bulb tube, which was then held at room temperature. Time-dependent IR spectra of the vaporized samples (Figure S6) revealed the formation of ClC(O)NCS; $OCCl_2$ (1827 and 849 cm^{-1}) and OCS (2062 cm^{-1})[33,34] were also detected. Time-dependent IR was appropriate to monitor the kinetics for the FC(O)SCN → FC(O)NCS isomerization;[9] however, in this case it was not suitable because the competitive channels are not negligible. On the other hand, ClC(O)SCN is stable in the gas phase at 100 °C, and its rearrangement to ClC(O)NCS is catalyzed in the liquid and on surfaces with traces of water.

Photoelectron Spectra. The He(I) photoelectron spectrum of ClC(O)SCN has been measured and depicted in Figure 13. The experimental and theoretical ionization energies are listed in Table 9, along with the assignments of occupied molecular orbitals. Both stable *syn* and *anti* forms adopt C_s symmetry, and the canonical molecular orbitals of type a′ are σ-orbitals lying

dx.doi.org/10.1021/jp400281g | J. Phys. Chem. A 2013, 117, 2383−2399

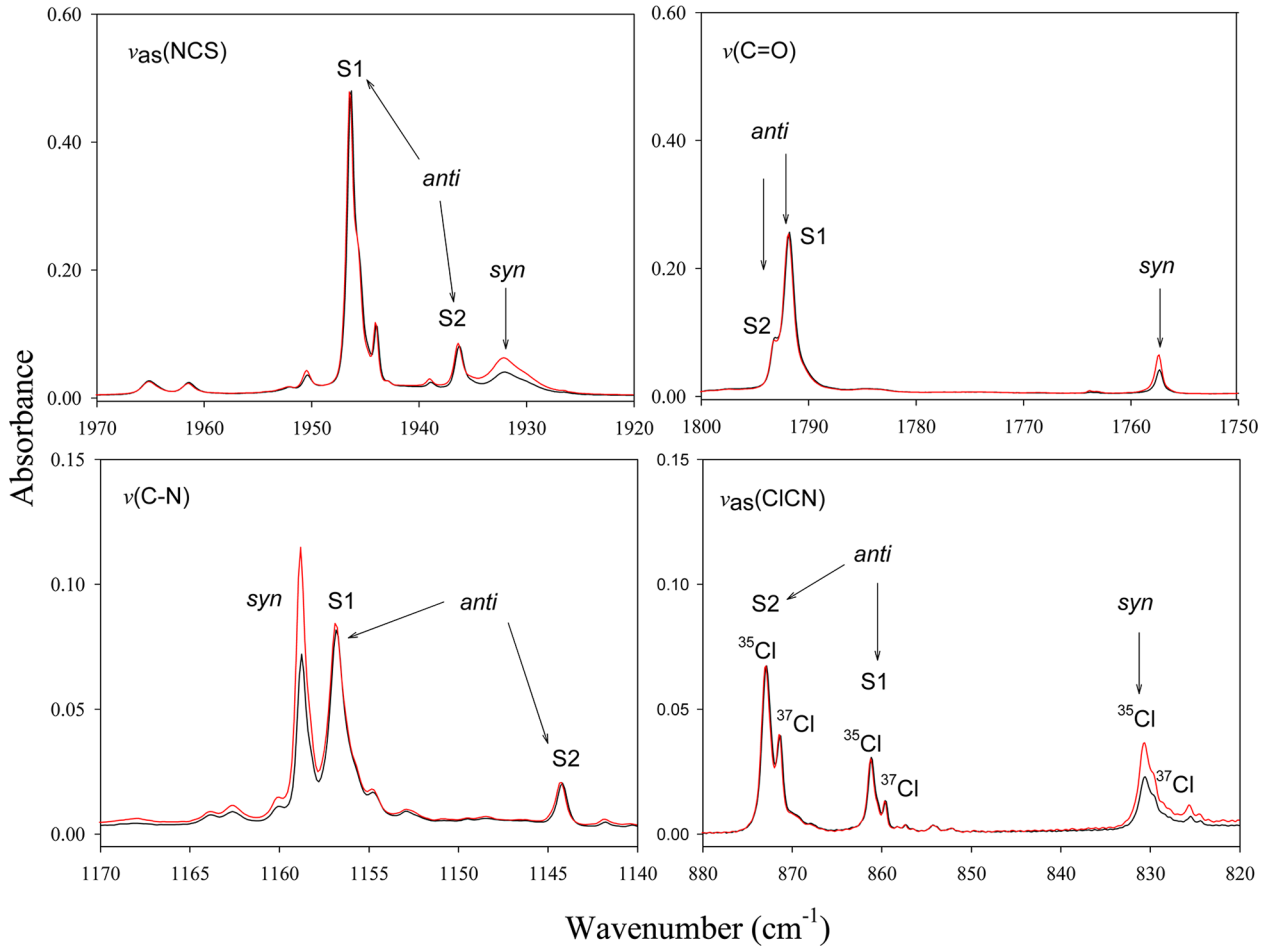

Figure 8. IR spectra of an equilibrium mixture of *syn* and *anti* ClC(O)NCS obtained at nozzle temperatures of 25 °C (black line) and 200 °C (red line) and deposited in solid argon at 15 K. Intensities are normalized to the ν(C═O) of *anti* ClC(O)NCS.

in the molecular plane, while those of type a″ are π-orbitals. The assignment of the PE spectrum bands to photoionization processes from specific molecular orbitals were made with reference to the results of Outer-Valence Green's Function (OVGF) and Symmetry Adapted Cluster/Configuration Interaction (SAC-CI) calculations using the triple-ξ quality 6-311+G* basis set at the fully optimized molecular geometry (B3LYP/6-311+G*) for both conformers. The characters of the highest occupied molecular orbital (HOMO) are shown in Figure S7 (Supporting Information).

The first ionization band appearing in the spectrum at 10.77 eV can be assigned with confidence to the ionization process from the HOMO, an n_π(S) orbital, which can be visualized as a lone pair nominally localized on the sulfur atom. The calculated values are in qualitative agreement with this assignment, although both OVGF and SAC-CI methods yield too high vertical ionization energy values: 10.98 and 11.11 eV, respectively. Due to resonance interactions present in the −SCN group, electron density contributions from the πC≡N bond can be also postulated. This resonance was found for related thiocyanate species, leading to a stabilization in the a″ n_π(S) HOMO orbital, with vertical ionization energies of 10.13, 10.39, 10.55, and 10.78 eV for CH_3SCN,[35] CH_2ClSCN, CCl_3SCN, and CCl_2FSCN, respectively.[36] Natural bond orbital (NBO) analysis indicates that the outermost orbital is of pure p-type with π symmetry, [lp_π(S)], with a low electron occupancy of 1.75 *e*, signifying the electron-donating capacity for this orbital. The main acceptor orbital is the π^*(C≡N) antibonding orbital, in perfect agreement with the previous picture. The strong stabilization found for the HOMO is assisted by the planarity of ClC(O)SCN, which favored electronic delocalization over the whole molecule. As commented before, this resonance effect also influences the conformational properties, and subtle differences in orbital stabilization are expected for both conformers. However, since the experimental resolution of the PES precludes the observation of minor differences in the ionization energy values arising from different conformations, the analysis is made with reference to the most stable *syn* form.

A second signal in the spectrum at 11.82 eV has a narrow and sharp contour, which is characteristic of ionization from essentially nonbonding orbitals. In comparison with the photoelectron spectra for related sulfenylcarbonyl compound,[37−39] this bands is associated primarily with the ionization of oxygen lone-pair electrons (n_O) of the −SC(O)− group, with a′ symmetry. In comparison with similar ClC(O)S-containing molecules,[40] the third band observed in the spectrum can be assigned to ionization from the chloride nonbonding orbitals of a″ and a′ symmetry, with contribution also from the $\pi_{C=O}$ orbital, as suggested by the high intensity displayed by this signal.

■ CONCLUSION

This work presents the synthesis and spectroscopic characterization of the constitutional isomers ClC(O)SCN and ClC(O)NCS. Both compounds exhibit *syn*/*anti* conformational

dx.doi.org/10.1021/jp400281g | J. Phys. Chem. A 2013, 117, 2383−2399

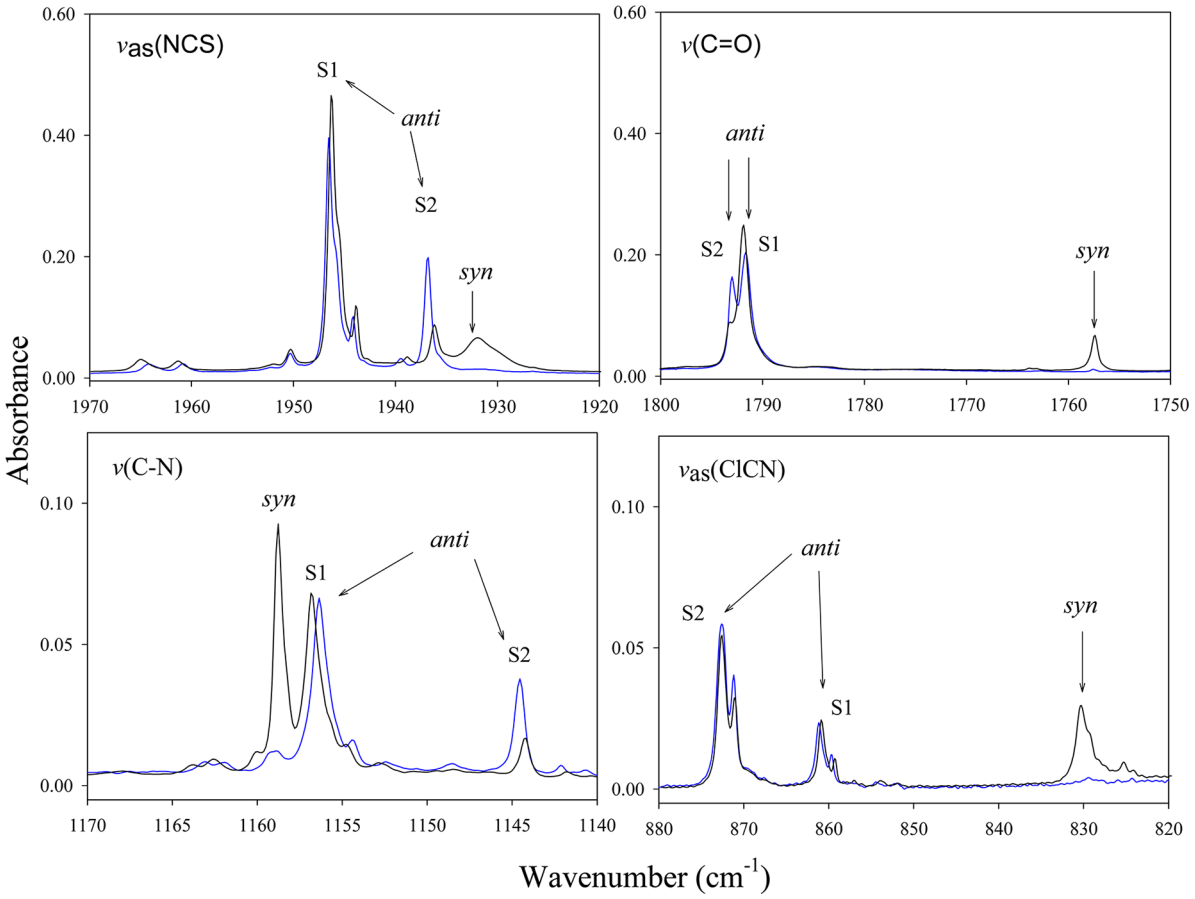

Figure 9. IR spectra of Ar-matrix isolated ClC(O)NCS at 15 K (black line) and after annealing the matrix to 35 K (blue trace).

Table 6. Rate Constants (k), Half-Life Times ($t_{1/2}$) and Activation Energies (E_a) for the *syn* → *anti* Rotational Isomerization of ClC(O)NCS in Solid Argon and Solid Nitrogen

T (K)	k^a ($\times 10^4$, s^{-1})	$t_{1/2}$ (min)	$E_a{}^a$ (kcal mol^{-1})
22.8	0.7 (0.1)	174.4	0.98 (0.15)
26.4	5.5 (0.3)	21.1	
28.0	18.4 (0.5)	6.3	
31.0	242.8 (26.1)	0.5	

[a]One standard deviation of the fit are given in parentheses.

equilibrium in the gas phase. The *syn* and *anti* planar forms (C_s symmetry) were calculated to be the most stable rotamers for the thiocyanate and isothiocyanate isomers, respectively, in good agreement with the observed vibrational spectra. The experimental *syn* ↔ *anti* enthalpy difference for ClC(O)SCN was determined to be ΔH_{exp} = 1.3 (0.3) kcal mol^{-1} by trapping the temperature-dependent gas-phase equilibrium composition in a solid Ar matrix at 15 K. Evaluation of ΔH_{exp} failed for ClC(O)NCS because of its small rotational barrier around the C−N single bond. Interestingly, the small barrier allowed us to study the *syn* → *anti* interconversion of ClC(O)NCS in argon matrices between 22 and 31 K. A rotational barrier of 0.98 (0.15) kcal mol^{-1} was determined by the temperature dependence of the exchange rates evaluated at cryogenic temperatures in Ar matrices. The experimental barrier is within the experimental uncertainties coincident with calculated values. On the other hand, the reversed *anti* → *syn* isomerization was achieved by photolysis of ClC(O)NCS isolated in solid argon at 15 K using UV−visible radiation.

Liquid ClC(O)SCN is unstable at room temperature and isomerizes to ClC(O)NCS along with competitive decomposition pathways, which leads mainly to the formation of $OCCl_2$ and OCS and a nonidentified orange solid. Rearrangement to ClC(O)NCS can also be induced by photolysis using broad-band UV−visible radiation. The main and common photoevolution channel corresponds to the CO extrusion of both constitutional isomers and the generation of the ClSCN species.

EXPERIMENTAL SECTION

Synthesis. ClC(O)SCN was synthesized by the reaction of chlorocarbonylsulfenyl chloride and excess of silver cyanide. ClC(O)SCl (8 mmol) was distilled onto dry AgCN (25 mmol) contained in an evacuated vessel provided with a Young valve and connected at the vacuum line. The reaction was carried out for 18 h from −10 to 10 °C. The purification of the product was performed by repeated trap-to-trap distillations at −50, −90, and −196 °C. ClC(O)SCN was isolated in the trap at −50 °C (solid) together with a small amount of the more volatile ClC(O)SCl (liquid), which was further separated by slow vacuum distillation. The final yield was around 30%.

ClC(O)NCS was obtained by decarbonylation of ClC(O)C(O)NCS, which was prepared from oxalyl chloride and silver thiocyanate. Thus, ClC(O)C(O)Cl (8 mmol) was distilled onto dry AgSCN (8 mmol) in a vessel provided with a Young valve. The mixture was kept at 0 °C for 15 h in a ice bath, the reaction vessel was warmed at room temperature, and 0.1 g of activated carbon was quickly added. Subsequently, the air was removed in

dx.doi.org/10.1021/jp400281g | J. Phys. Chem. A 2013, 117, 2383−2399

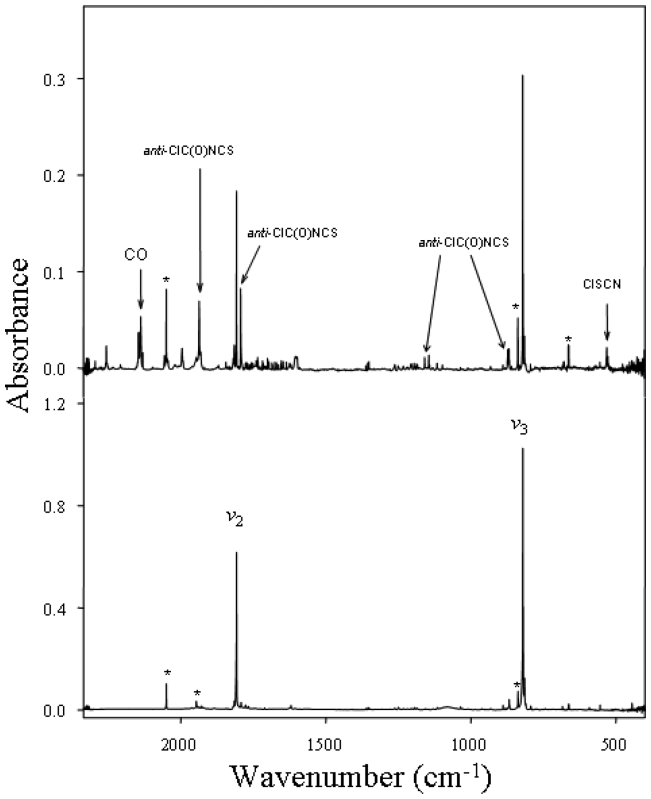

Figure 10. IR spectrum of Ar-matrix-isolated ClC(O)SCN recorded before (lower trace) and after (upper trace) 30 min photolysis using broad-band UV−visible radiation. *Impurity bands.

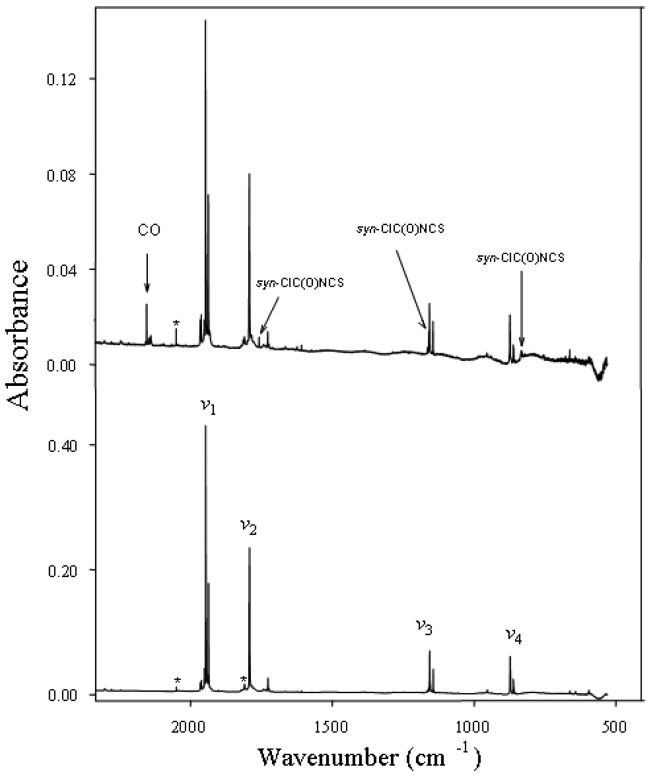

Figure 11. IR spectrum of Ar-matrix-isolated ClC(O)NCS recorded before (lower trace) and after (upper trace) 13 min of photolysis using broad-band UV−visible radiation. *Impurity bands.

Table 7. Frequencies, Intensities and Assignments of IR Absorption Bands Produced after 30 min of UV−Visible Broad Band Irradiation of Ar-Matrix Isolated ClC(O)SCN at 15 K

IR (Ar-matrix)		Assignment		Previously
ν (cm^{1})	I^a	Molecule	Vibrational Mode	Reported Values
2294.8	0.015 (4)	-		
2256.4	0.081 (22)	-		
2207.8	0.015 (4)	-		
2145.9		CO····complexed		
2144.7				
2140.6	0.364 (100)		ν(C≡O)	2138.6[b]
2137.9		CO		
2130.9				
2056.2	0.022 (6)	-		
1995.5	0.093 (26)	-		
1936.3	0.303 (83)	*anti*-ClC(O)NCS	ν_{as}(NCS)	1936.3[c]
1930.9		*syn*-ClC(O)NCS	ν_{as}(NCS)	1931.9[c]
1793.3	0.170 (47)	*anti*-ClC(O)NCS	ν(C=O)	1793.1[c]
1757.3	0.012 (3)	*syn*-ClC(O)NCS	ν(C=O)	1757.4[c]
1158.8	0.017 (5)	*syn*-ClC(O)NCS	ν(C–N)	1158.8[c]
1144.4	0.029 (8)	*anti*-ClC(O)NCS	ν(C–N)	1144.2[c]
1097.5	-	-		
872.5	0.046 (13)	*anti*-ClC(O)NCS	ν_{as}(Cl-C-N)	872.9[c]
830.4	0.012 (3)	*syn*-ClC(O)NCS	ν_{as}(Cl-C-N)	830.7[c]
680.0	0.017 (5)	ClSCN	ν(S–C)	678.9[d]
677.3				
530.7	0.040 (11)	ClSCN	ν(Cl–S)	533.6[d]
526.8	0.016 (4)			

[a]Integrated absorbances and relative intensity between parentheses. [b]Reference 30. [c]This work. [d]Reference 24.

vacuum, and the mixture was heated at 80 °C for 6 h. The products were separated by trap-to-trap distillation keeping the traps at −33, −90, and −196 °C. The ClC(O)NCS was retained in the −33 °C trap with a yield of around 80%. The purities of ClC(O)SCN and ClC(O)NCS were checked by IR, Raman, UV, and ^{13}C NMR spectroscopy.

Isomerization Experiments. The rearrangement of chlorocarbonyl thiocyanate, ClC(O)SCN, into chlorocarbonyl isothiocyanate, ClC(O)NCS, was studied in the gas and liquid phases. For the gas phase experiments, 2 mbar of ClC(O)SCN was placed into an IR gas cell and keep at different temperatures from 25 to 100 °C. IR spectra were recorded at different times (0−12 h) to follow the isomerization. For liquid phase studies small amounts of ClC(O)SCN (5 mg) were condensed in a small

dx.doi.org/10.1021/jp400281g | J. Phys. Chem. A 2013, 117, 2383−2399

Table 8. Frequencies, Intensities, and Assignments of IR Absorption Bands Produced after 13 min of UV−Visible Irradiation of Ar-Matrix Isolated ClC(O)SCN at 15 K

IR (Ar matrix)		Assignment		Previously
ν (cm^{-1})	I^a	Molecule	Vibrational Mode	Reported Values
2153.9	0.0142	CO···complexed		
2145.9				
2141.1			ν(C≡O)	2138.6[b]
	0.0144	CO		
2139.0				
2137.4				
1932.4	-	*syn*-ClC(O)NCS	ν_{as}(NCS)	1931.9[c]
1757.4	0.0051	*syn*-ClC(O)NCS	ν(C=O)	1757.4[c]
1158.7	-	*syn*-ClC(O)NCS	ν(C–N)	1158.8[c]
830.7	0.0079	*syn*-ClC(O)NCS	ν_{as}(Cl-C-N)	830.7[c]
676.6		ClSCN	ν(S–C)	678.9[d]

[a]Integrated absorbances. [b]Reference 30. [c]This work. [d]Reference 24.

vessel adapted to a vacuum line, which was connected to an IR gas cell. This vessel was kept at 25 °C, and IR spectra of vaporized samples were recorded at different times (0−3 h).

Instrumentation. *(a). General Procedure.* Volatile materials were manipulated in a glass vacuum line equipped with a capacitance pressure gauge, three U-traps, and valves with PTFE stems. The vacuum line was connected to an IR cell (optical path length 200 mm, Si windows 0.5 mm thick) placed in the sample compartment of a FTIR spectrometer. This arrangement allowed following the course of the reactions and the purification processes. The pure compounds were stored in flame-sealed glass ampules under liquid nitrogen in a Dewar vessel. The ampules were opened with an ampule key[41] at the vacuum line, an appropriated amount was taken out for the experiments, and

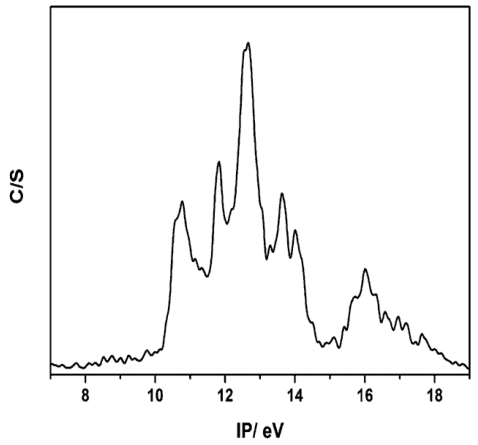

Figure 13. He(I) photoeletron spectrum of ClC(O)SCN.

Table 9. Experimental and Calculated Ionization Energies (eV) and MO Characters for *syn*-ClC(O)SCN

	$IP_{cal}{}^{a,b}$			
IP_{exp}	OVGF/6-311+G*	SAC−CI/6-311+G*	MO	symmetry/ character
10.77	10.98 (0.91)	11.11 (0.94)	30	a″/n_S, $\pi_{C\equiv N}$
11.82	12.12 (0.91)	11.85 (0.94)	29	a′/n_O, n_S, n_{Cl}
12.63	12.74 (0.91)	12.85 (0.94)	28	a′/n_{Cl}, $\pi_{C\equiv N}$
	12.76 (0.91)	12.92 (0.95)	27	a″/n_{Cl}, $\pi_{C=O}$
13.62	13.40 (0.90)	13.64 (0.94)	26	a′/n_O, n_{Cl}, $\pi_{C\equiv N}$
13.99	14.10 (0.90)	14.04 (0.91)	25	a′/$\sigma_{C\equiv N}$
14.44	14.43 (0.91)	14.29 (0.92)	24	a′/n_S, σ_{C-S}
15.98	16.10 (0.90)	16.14 (0.94)	23	a″/π_{SCN}
16.59	16.72 (0.88)	16.62 (0.88)	22	a″/$\pi_{C=O}$

[a]Geometry computed at the B3LYP/6-311+G* level of approximation. [b]Pole strength (OVGF) and intensities (SAC-CI) are given in parentheses.

then they were flame-sealed again. The vapor pressures of the samples were measured in a small vacuum line equipped with a calibrated capacitance pressure gauge and a small sample reservoir. The melting point was determined using small

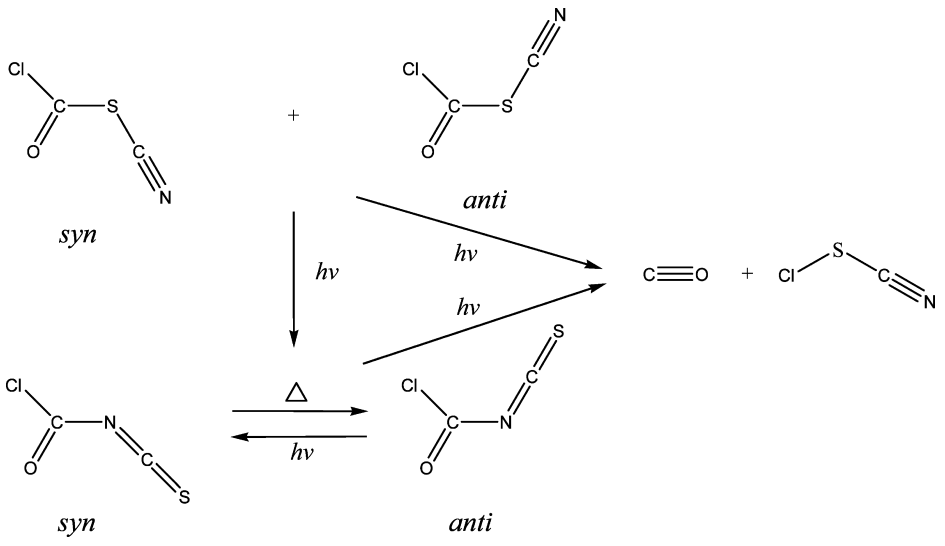

Figure 12. Summary of the thermal (Δ) and photochemical ($h\nu$) isomerization reactions, as well as of the photodecomposition observed for ClC(O)SCN and ClC(O)NCS isolated in solid Ar.

dx.doi.org/10.1021/jp400281g | J. Phys. Chem. A 2013, 117, 2383−2399

amounts of the samples contained in a 4 mm glass tube immersed in a cold bath in a transparent Dewar vessel.

(b). Vibrational Spectroscopy. Infrared gas spectra were recorded with a resolution of 2 cm^{-1} in the range from 4000 to 400 cm^{-1}, using a glass cell with Si windows and an optical path length of 200 mm. Raman spectra of the neat liquid (room temperature) and of solid samples (cooled with nitrogen gas) were measured in flame-sealed capillaries (3 mm o.d.) with a 1064 nm Nd:YAG laser, in the region from 4000 to 100 cm^{-1} at a resolution of 2 cm^{-1}.

(c). Matrix Isolation Experiments. For matrix isolation experiments a few milligrams of ClC(O)SCN were transferred to a small U-trap connected to the inlet nozzle of the matrix apparatus. A gas stream of argon (2 mmol h^{-1}) was directed over the sample held at −65 °C, and the resulting gas mixture was condensed onto the cold matrix support (15 K, Rh plated Cu block) in a high vacuum. The thermally more stable ClC(O)-NCS was mixed with argon in a ratio of 1:4000 in a 1 L stainless-steel storage container, and then small amounts of the mixture were deposited within 10 min on the cold matrix support at 15 K.

Temperature-dependent experiments were carried out by passing the gaseous sample-Ar mixtures through a quartz nozzle (1 mm i.d.), heated over a length of ≈10 mm with a platinum wire (0.25 mm o.d.) prior to deposition on the matrix support. The nozzle was held at 103 and 210 °C for ClC(O)SCN and at 200 and 320 °C for ClC(O)NCS. Photolysis experiments were performed using broad-band UV−visible radiation ($200 < \lambda < 800$ nm) passed through a water-cooled quartz lenses to prevent heating effects. The radiation was provided by a high-pressure mercury lamp, and the accumulated irradiation times for ClC(O)SCN and ClC(O)NCS were 20 and 13 min, respectively.

IR spectra of matrix isolated samples were recorded in a reflectance mode using a transfer optic. An MCT detector and a KBr/Ge beam splitter were used in the wavenumber range 5000−530 cm^{-1}. For the spectra with apodized resolutions of 0.25 cm^{-1}, 200 scans (few scans in annealing measurements) were added. More details of the matrix apparatus are given elsewhere.[42]

Annealing experiments were performed on deposits of ClC(O)NCS isolated in solid argon, prepared as described above at 15 K. The deposit was then allowed to warm up and held at a certain temperature in the range from 22.0 to 31.0 K. For kinetic measurements, the temperature was kept constant to about ±0.3 K, and the uncertainty of the deposit temperature measurement was about 1 K. At each temperature, spectral changes were monitored by several sequent recorded IR spectra.

Experiments on ClC(O)SCN were also performed using a gas mixture of the sample in argon (1:1000) in a 1 L glass storage container. The mixture was deposited on a CsI window cooled at 16 K by means of a Displex closed-cycle refrigerator using the pulse deposition technique. IR spectra of each matrix sample were recorded at resolution of 0.5 cm^{-1}, with 64 scans, using MCTB and DTGS detectors for the ranges 4000−400 or 600−180 cm^{-1}, respectively. For photolysis experiments of ClC(O)-SCN, the matrix was exposed to a broad-band UV−visible radiation ($200 \le \lambda \le 800$ nm) from a Hg−Xe arc lamp operating at 1000 W, using a water filter in the output to absorb IR radiation and to minimize any heating effects. The accumulated irradiation time was 120 min.

(d). UV Spectroscopy. UV−visible spectra of the gas phase of ClC(O)SCN and ClC(O)NCS were recorded using a glass cell equipped with quartz windows (10 cm optical path length). Measurements were carried out in the spectral region from 190 to 700 nm with a sampling interval of 1.0 nm, a scan speed of 200 nm min^{-1}, and a slit width of 2 nm.

(e). NMR Spectroscopy. For ^{13}C NMR measurements, pure samples were flame-sealed in thin-walled 4 mm o.d. tubes and placed into 5 mm NMR tubes. The NMR spectra were recorded at 100.6 MHz. The samples were held at 0 °C and CD_3OD was used as an external lock and reference.

(f). Quantum Chemical Calculations. Quantum chemical calculations were performed using the program package GAUSSIAN 03.[43] Scans of the potential energy surface, structure optimizations and vibrational frequencies of various isomers of ClC(O)SCN have been carried out applying ab initio (MP2),[44] density functional theory (B3LYP),[45−48] and complete basis set CBS-QB3 methods.[49,50] TSs for the unimolecular isomerization of ClC(O)SCN to ClC(O)NCS and for their internal *syn*−*anti* rotational interconversion were optimized by the Synchronous Transit-guided Quasi-Newton (STQN) method implemented by Schlegel and co-workers,[51] and barrier heights were calculated from the energies of the TS and the stable structures, taking into account zero-point vibrational energies. The SAC-CI[52] and OVGF[53,54] calculations were applied to determine the ionization energies for both conformers, using the 6-311+G* basis set and B3LYP/aug-cc-pVTZ optimized geometry. Coupled-cluster CCSD(T)[55] analytical gradient-based geometry optimizations were performed with the CFOUR program.[56]

(g). Photoelectron Spectroscopy. The HeI PE spectrum of ClC(O)SCN was recorded on a double-chamber UPS-II machine built specifically to detect transient species at a resolution of about 30 meV, as indicated by the $Ar^+(^2P_{3/2})$ photoelectron band.[57−59] Experimental vertical ionization energies (I_v in eV) were calibrated by simultaneous addition of a small amount of argon and iodomethane to the sample.

(h). Crystal Growth and Transfer. A small amount (ca. 10 mg) of ClC(O)SCN was condensed (−196 °C) in vacuum into the upper part of a glass tube (o.d.: 6 mm, length 15 cm), which was equipped with a valve and a PTFE stem. The lower part of the tube (ca. 5 cm) was immersed in a cold ethanol bath at −20 °C within a stainless steel Dewar, while the upper part was maintained inside the Dewar but above the cooling liquid. Three hours later, colorless crystals were observed on the inner wall of lower part of the container. The vessel containing the crystals was cooled with dry ice, and the valve was slowly opened to 1 atm. of argon gas. The lower part of the container (ca. 5 cm) was carefully scratched with a glass cutter and carefully broken. Then the tube containing crystals was quickly moved into a trough that was precooled by a flow of cold nitrogen gas (−40 °C). Suitable crystals were subsequently selected under the microscope and mounted as previously described.[60]

(i). X-ray Crystallography. Crystal was mounted on a diffractometer, equipped with a 2K × 2K EOS CCD area detector, a four-circle kappa goniometer, and sealed-tube Enhanced (Mo) and an Enhanced Ultra (Cu) sources. For data collections, a Cu source emitting monochromated Cu−Kα radiation (λ = 1.54184 Å) was used. The diffractometer was controlled by the *CrysAlis*^{Pro} Graphical User Interface software.[61] The diffraction data collection strategy was optimized with respect to complete coverage and consisted of 10 ω scans with a width of 1°, respectively. The data collection was carried out at −123 °C, in a 1024 × 1024 pixel mode using 2 × 2 pixel binning. Processing of the raw data, scaling of diffraction data, and the application of an empirical absorption correction was completed by using the *CrysAlis*^{Pro} program.[61] The solution of the structure was obtained by direct methods that located the positions of all

atoms. The final refinement was obtained by introducing anisotropic thermal parameters and the recommended weightings for all atoms. All calculations were performed using the *WinGX v1.64.05* package program for the structure determination, solution refinement, and molecular graphics.[62,63] Crystal structure data have been deposited at the Cambridge Crystallographic Data Centre (CCDC). Enquiries for data can be direct to: Cambridge Crystallographic Data Centre, 12 Union Road, Cambridge, UK, CB2 1EZ or (e-mail) deposit@ccdc.cam.ac.uk or (fax) +44 (0) 1223 336033. Any request to the CCDC for this material should quote the full literature citation and the reference number 915247.

(j). Gas Electron Diffraction of ClC(O)NCS. The electron diffraction patterns were recorded on the heavily improved Balzers Eldigraph KD-G2 gas-phase electron diffractometer at the University of Bielefeld.[64] The experimental details are presented in Table 10. In total, three images for each, the long and short nozzle-to-plate distances, were measured on imaging plates. The plates with the diffraction patterns were scanned using a calibrated scanner. The intensity curves (Figure S8 and S9) were obtained by applying the method described earlier.[65] Sector function and electron wavelengths were calibrated using benzene diffraction patterns, recorded along with the substance under investigation.[66] In order to compute vibrational mean square amplitudes and curvilinear corrections to equilibrium structure for all interatomic distances used in the gas-phase electron diffraction refinements, analytical quadratic and numerical cubic force fields were calculated for both *anti* and *syn* conformers employing the MP2(full)/cc-pVTZ approximation. The amplitudes and corrections were then calculated with the SHRINK program.[67−69] Experimental amplitudes were refined in groups (see Tables S5 and S6). For this purpose, the scale factors (one per group) were used as independent parameters. Thus, the ratios between different amplitudes in one group were fixed at the theoretical values. In order to avoid the influence of the outliers in experimental scattering data, we applied a method of adjusting weights in the final stages of refinement.[70] The final parameters refined in this way (see Table 3) were insignificantly shifted with respect to those obtained with fixed weights equal to 1.0. The final structural *R*-factor after the adjustment of weights was 5.9%.

Table 10. Experimental Details of the GED Experiment

parameter	short camera distance	long camera distance
nozzle-to-plate distance/mm	250.0	500.0
accelerating voltage/kV	60	60
fast electrons current/μA	1.03	0.9
electron wavelength[a]/Å	0.048626	0.048518
nozzle temperature/K	274	277
residual gas pressure[b]/mbar	2×10^{-6}	2×10^{-6}
exposure time/sec	13	15
used *s* range/Å^{-1}	6.4−32.0	2.2−16.0
number of inflection points[c]	7	5

[a]Determined from C_6H_6 diffraction patterns measured in the same experiment. [b]During the measurement. [c]Number of inflection points on the background line.

■ ASSOCIATED CONTENT

Supporting Information

Calculated structural parameters of ClC(O)SCN (Table S1), calculated structural parameters of ClC(O)NCS (Table S2), vapor pressure curve and Claussius-Clapeyron plot of ClC(O)-NCS (Figure S1), ^{13}C NMR spectrum of ClC(O)SCN (Figure S2), UV−visible spectrum of gaseous ClC(O)SCN and ClC(O)NCS (Figure S3). The crystal packing is shown in Figure S4. Arrehnius plot obtained for the *syn* → *anti* interconversion of ClC(O)NCS isolated in Ar matrix in the temperature range of 22−31 K (Figure S5), IR spectra (gas) of the ClC(O)SCN to ClC(O)NCS isomerization in the liquid phase at 25 °C (Figure S6). Characters of the highest occupied molecular orbital are shown in Figure S7. Total electron diffraction intensity curves and additive background lines are shown in Figure S8. Experimental and model electron diffraction molecular intensity curves are shown in Figure S9. Crystallographic information file in CIF format is also furnished. This material is available free of charge via the Internet at http://pubs.acs.org/.

■ AUTHOR INFORMATION

Corresponding Author

*Tel/Fax ++54-221-425-9485. E-mail: carlosdv@quimica.unlp.edu.ar.

Notes

The authors declare no competing financial interest.

■ ACKNOWLEDGMENTS

The Argentinean authors thank the Agencia Nacional de Promoción Científica y Técnica (ANPCYT), Consejo Nacional de Investigaciones Científicas y Técnicas (CONICET), Comisión de Investigaciones de la Provincia de Buenos Aires (CIC), Facultad de Ciencias Exactas, Universidad Nacional de La Plata (UNLP), and Departamento de Ciencias Básicas de la Universidad Nacional de Luján for financial support. L.A.R. gratefully acknowledges the DAAD, UNLP and Bergische Universität Wuppertal. C.O.D.V. acknowledges the DAAD, which generously sponsors the DAAD Regional Program of Chemistry for the Argentina supporting Latin-American students to do their Ph.D. in La Plata. C.O.D.V. and N.W.M. are grateful to Deutsche Forschungsgemeinschaft for support through an international project. Y.V.V. acknowledges the Humboldt Foundation for a fellowship. H.B. and H.W. acknowledge the support from the Deutsche Forschungsgemeinschaft and the Fonds der Chemischen Industrie.

■ REFERENCES

(1) Carsten, C. Acyl Thiocyanates. I. Aroyl Thiocyanates. *Acta Chem. Scand.* **1971**, *25*, 1160−1162.

(2) Carsten, C. Acyl Thiocyanates. II. Aralkanoyl, Alkanoyl, and 2-Alkenoyl Thiocyanates. *Acta Chem. Scand.* **1971**, *25*, 1162−1164.

(3) Haas, A.; Reinke, H. Halogenocarbonylschwefel-Pseudohalogenide. *Angew. Chem.* **1967**, *79*, 687−688.

(4) Haas, A.; Reinke, H.; Pseudohalogenverbindungen, X. I. I. Halogencarbonylsulfenyl-Pseudohalogenide. *Chem. Ber.* **1969**, *102*, 2718−2727.

(5) Koch, R.; Finnerty, J. J.; Wentrup, C. Rearrangements and Interconversions of Heteroatom-Substituted Isocyanates, Isothiocyanates, Nitrile Oxides, and Nitrile Sulfides, RX-NCY and RY-CNX. *J. Org. Chem.* **2011**, *76*, 6024−6029.

(6) Koch, R.; Finnerty, J. J.; Murali, S.; Wentrup, C. [3,3]-Sigmatropic Shifts and Retro-ene Rearrangements in Cyanates, Isocyanates, Thiocyanates, and Isothiocyanates of the Form RX-YCN and RX-NCY. *J. Org. Chem.* **2012**, *77*, 1749−1759.

(7) Koch, R.; Wentrup, C. Rearrangements of Acyl, Thioacyl, and Imidoyl (Thio)cyanates to Iso(thio)cyanates, Acyl Iso(thio)cyanates to (Thio)acyl Isocyanates, and Imidoyl Iso(thio)cyanates to (Thio)acyl

Carbodiimides, RCX-YCN ⇌ RCX-NCY ⇌ RCY-NCX ⇌ RCY-XCN (X and Y = O, S, NR′). *J. Org. Chem.* **2013**, DOI: 10.1021/jo3013786.
(8) Torrico-Vallejos, S.; Erben, M. F.; Ge, M.-F.; Willner, H.; Della Védova, C. O. Conformational Behavior of $CH_3OC(O)SX$ (X = CN and SCN) Pseudohalide Congeners. A Combined Experimental and Theoretical Study. *J. Phys. Chem. A* **2010**, *114*, 3703−3712.
(9) Ramos, L. A.; Ulic, S. E.; Romano, R. M.; Erben, M. F.; Lehmann, C. W.; Bernhardt, E.; Beckers, H.; Willner, H.; Della Védova, C. O. Vibrational Spectra, Crystal Structures, Constitutional and Rotational Isomerism of FC(O)SCN and FC(O)NCS. *Inorg. Chem.* **2010**, *49*, 11142−11157.
(10) Bunnenberg, R.; Jochims, J. C. Oxalyl-isothiocyanate und Carbonyl-halogenid-isothiocyanate. *Chem. Ber.* **1981**, *114*, 1746−1751.
(11) Alleres, D. R.; Cooper, D. L.; Cunningham, T. P.; Gerratt, J.; Karadakov, P. B.; Raimondi, M. Bonding in YXXY Dihalides and Dihydrides of Dioxygen and Disulfur. *J. Chem. Soc., Faraday Trans.* **1995**, *91*, 3357−3362.
(12) Erben, M. F.; Della Védova, C. O.; Romano, R. M.; Boese, R.; Oberhammer, H.; Willner, H.; Sala, O. Anomeric and Mesomeric Effects in Methoxycarbonylsulfenyl Chloride, $CH_3OC(O)SCl$: An Experimental and Theoretical Study. *Inorg. Chem.* **2002**, *41*, 1064−1071.
(13) Romano, R. M.; Della Védova, C. O.; Downs, A. J.; Parson, S.; Smith, C. Structural and Vibrational Properties of ClC(O)SY Compounds with Y = Cl and CH_3. *New J. Chem.* **2003**, *27*, 514−519.
(14) Rodriguez Pirani, L.; Erben, M. F.; Boese, R.; Pozzi, C. G.; Fantoni, A. C.; Della Védova, C. O. Conformational Preference of Chlorothioformate Species: Molecular Structure of Ethyl Chlorothioformate, $ClC(O)SCH_2CH_3$ in the Solid Phase and NBO Analysis. *Acta Crystallogr.* **2011**, *B67*, 350−356.
(15) Bondi, A. van der Waals Volumes and Radii. *J. Phys. Chem.* **1964**, *68*, 441−451.
(16) Nakata, M.; Kohata, K.; Fukuyama, T.; Kuchitsu, K. Molecular Structure of Phosgene as Studied by Gas Electron Diffraction and Microwave Spectroscopy: The r_z Structure and Isotope Effect. *J. Mol. Spectrosc.* **1980**, *83*, 105−117.
(17) Groner, P.; Warren, R. D. Approximate r_e Structures from Experimental Rotational Constants and Ab Initio Force Fields. *J. Mol. Struct.* **2001**, *599*, 323−335.
(18) Yamada, K.; Winnewisser, M.; Winnewisser, G.; Szalanski, L. B.; Gerry, M. C. L. Ground State Spectroscopic Constants of $H^{15}NCS$, $HN^{13}CS$, and $HNC^{34}S$, and the Molecular Structure of Isothiocyanic Acid. *J. Mol. Spectrosc.* **1980**, *79*, 295−313.
(19) Cradock, S.; Durig, J. R.; Sullivan, J. F. Electron Diffraction Investigation of the Molecular Structures of Ethyl Isocyanate and Ethyl Isothiocyanate. *J. Mol. Struct.* **1985**, *131*, 121−130.
(20) Erben, M. F.; Padró, J. M.; Willner, H.; Della Védova, C. O. Conformational and Structural Determination of $F_2NC(O)F$ and $F_2NC(O)NCO$. A Joint Experimental and Theoretical Study. *J. Phys. Chem. A* **2009**, *113*, 13029−13035.
(21) Della Védova, C. O.; Cutín, E. H.; Varetti, E. L.; Aymonino, P. J. Infrared and Raman Spectra and Force Constants of Chlorocarbonylsulfenyl Chloride, ClC(O)SCl. *Can. J. Spectrosc.* **1984**, *29*, 69−74.
(22) Romano, R. M.; Della Védova, C. O.; Downs, A. J.; Greene, T. M. Matrix Photochemistry of *syn*-(Chlorocarbonyl)sulfenyl Bromide, *syn*-ClC(O)SBr: Precursor to the Novel Species *anti*-ClC(O)SBr, *syn*-BrC(O)SCl, and BrSCl. *J. Am. Chem. Soc.* **2001**, *123*, 5794−5801.
(23) Della Védova, C. O.; Haas, A. Synthese und Charakteresierung von Halogencarbonuylmercapto-Verbindungen. *Z. Anorg. Allg. Chem.* **1991**, *600*, 145−151.
(24) Ulic, S. E.; Coyanis, E. M.; Romano, R. M.; Della Védova, C. O. *S*-Ethyl Thiochloroformate, $ClC(O)SCH_2CH_3$: Unusual Conformational Properties? *Spectrochim. Acta* **1998**, *A54*, 695−705.
(25) Campbell, N. L.; Gillis, C. J.; Klapstein, D.; Nau, W. M.; Balfour, W. J.; Fougère, S. G. Vibrational Spectra and Conformational Behaviour of Carbonyl Isothiocyanates X−CO−NCS, X = F, Cl, Br, MeO, EtO, and Acetyl isothiocyanate CH_3−CO−NCS. *Spectrochim. Acta* **1995**, *51A*, 787−798.
(26) Bodenbinder, M.; Ulic, S. E.; Willner, H. A Gas-Phase and Matrix Isolation Study of the Equilibrium CH_3ONO (Cis) ⇄ CH_3ONO (Trans) by FTIR Spectroscopy. *J. Phys. Chem.* **1994**, *98*, 6441−6444.
(27) Erben, M. F.; Della Védova, C. O.; Willner, H.; Trautner, F.; Oberhammer, H.; Boese, R. Fluoroformyl Trifluoroacetyl Disulfide, $FC(O)SSC(O)CF_3$: Synthesis, Structure in Solid and Gaseous States, and Conformational Properties. *Inorg. Chem.* **2005**, *44*, 7070−7077.
(28) Pettersson, M.; Maçôas, E. M. S.; Khriachtchev, L.; Lundell, J.; Fausto, R.; Räsänen, M. Cis → Trans Conversion of Formic Acid by Dissipative Tunneling in Solid Rare Gases: Influence of Environment on the Tunneling Rate. *J. Chem. Phys.* **2002**, *117*, 9095−9098.
(29) Pong, R.; Goldfarb, T. D.; Krantz, A. Kinetic Studies in Various Matrix - Probing the Host−Guest Interaction. *Ber. Bunsenges Phys. Chem.* **1978**, *82*, 9−10.
(30) Dubost, H. Infrared Absorption Spectra of Carbon Monoxide in Rare Gas Matrices. *Chem. Phys.* **1976**, *12*, 139−151.
(31) Durig, J. R.; Zheng, C.; Deeb, H. On the Structural Parameters and Vibrational Spectra of Some XNCS and XSCN (X = H, F, Cl, Br) Molecules. *J. Mol. Struct.* **2006**, *784*, 78−92.
(32) Devore, T. C. The Infrared Spectra of the Halogen Isocyanate and Thiocyanate Vapor Molecules. *J. Mol. Struct.* **1987**, *162*, 287−304.
(33) Frank, D. V.; Eugene, R. N. Infrared Spectra of Crystalline and Matrix-Isolated Carbonyl Sulfide. *J. Chem. Phys.* **1966**, *44*, 43−48.
(34) Lang, V. I.; Winn, J. S. Matrix-Isolated OCS: The High Resolution Infrared Spectra of a Cryogenically Solvated Linear Molecule. *J. Chem. Phys.* **1991**, *94*, 5270−5274.
(35) Pasinszki, T.; Veszprèmi, T.; Fehèr, M.; Kovaè, B.; Klasinc, L.; McGlynn, S. P. The Photoelectron Spectra of Methyl Pseudohalides. *Int. J. Quantum Chem.* **1992**, *44*, 443−453.
(36) Rodríguez Pirani, L. S.; Geronés, M.; Della Védova, C. O.; Romano, R. M.; Fantoni, A.; Cavasso-Filho, R.; Ma, C.; Ge, M.; Erben, M. F. Electronic Properties and Dissociative Photoionization of Thiocyanates. Part II. Valence and Shallow-Core (Sulfur and Chlorine 2p) Regions of Chloromethyl Thiocyanate, CH_2ClSCN. *J. Phys. Chem. A* **2012**, *116*, 231−241.
(37) Erben, M. F.; Della Védova, C. O. Dramatic Changes in Geometry After Ionization: Experimental and Theoretical Studies on the Electronic Properties of Fluorocarbonyl (Mono-, Di-, and Tri-) Sulfur Compounds. *Inorg. Chem.* **2002**, *41*, 3740−3748.
(38) Geronés, M.; Downs, A. J.; Erben, M. F.; Ge, M.; Romano, R. M.; Yao, L.; Della Védova, C. O. HeI Photoelectron and Valence Synchrotron Photoionization Studies of the Thioester Molecule $CH_3C(O)SCH_3$: Evidence of Vibronic Structure. *J. Phys. Chem. A* **2008**, *112*, 5947−5953.
(39) Geronés, M.; Erben, M. F.; Romano, R. M.; Della Védova, C. O.; Yao, L.; Ge, M. He I Photoelectron Spectra and Valence Synchrotron Photoionization for XC(O)SCl (X = F, Cl) Compounds. *J. Phys. Chem. A* **2008**, *112*, 2228−2234.
(40) Rodríguez Pirani, L. S.; Erben, M. F.; Geronés, M.; Ma, C.; Ge, M.; Romano, R. M.; Cavasso Filho, R. L.; Della Védova, C. O. Outermost and Inner-Shell Electronic Properties of $ClC(O)SCH_2CH_3$ Studied Using HeI Photoelectron Spectroscopy and Synchrotron Radiation. *J. Phys. Chem. A* **2011**, *115*, 5307−5318.
(41) Gombler, W.; Willner, H. Method for Opening and Resealing Glass Ampoules Several Times Under Sustained Vacuum. *J. Phys. E* **1987**, *20*, 1286−1288.
(42) Schnöckel, H.; Willner, H. *Matrix-Isolated Molecules*; VCH: Weinheim, Germany, 1994.
(43) Frisch, M. J.; Trucks, G. W.; Schlegel, H. B.; Scuseria, G. E.; Robb, M. A.; Cheeseman, J. R.; Montgomery Jr., J. A.; Vreven, T.; Kudin, K. N.; Burant, J. C.; et al. *Gaussian 03*, revision B.04 ed.; Gaussian, Inc.: Pittsburgh, PA, 2003.
(44) Møller, C.; Plesset, M. S. Note on an Approximation Treatment for Many-Electron Systems. *Phys. Rev.* **1934**, *46*, 618−622.
(45) Becke, A. D. Density-Functional Thermochemistry. III. The Role of Exact Exchange. *J. Chem. Phys.* **1993**, *98*, 5648−5652.
(46) Lee, C.; Yang, W.; Parr, R. G. Development of the Colle−Salvetti Correlation-Energy Formula into a Functional of the Electron Density. *Phys. Rev. B* **1988**, *37*, 785−789.

(47) Perdew, J. P.; Burke, K.; Ernzerhof, M. Generalized Gradient Approximation Made Simple. *Phys. Rev. Lett.* **1996**, *77*, 3865−3868.
(48) Perdew, J. P.; Burke, K.; Ernzerhof, M. Generalized Gradient Approximation Made Simple [Phys. Rev. Lett. 77, 3865 (1996)]. *Phys. Rev. Lett.* **1997**, *78*, 1396−1396.
(49) Montgomery, J. A., Jr.; Frisch, M. J.; Ochterski, J. W.; Petersson, G. A. A Complete Basis Set Model Chemistry. VII. Use of the Minimum Population Localization Method. *J. Chem. Phys.* **2000**, *112*, 6532−6542.
(50) Montgomery, J. J. A.; Frisch, M. J.; Ochterski, J. W.; Petersson, G. A. A Complete Basis Set Model Chemistry. VI. Use of Density Functional Geometries and Frequencies. *J. Chem. Phys.* **1999**, *110*, 2822−2827.
(51) Peng, C.; Ayala, P. Y.; Schlegel, H. B.; Frisch, M. J. Using Redundant Internal Coordinates to Optimize Equilibrium Geometries and Transition States. *J. Comput. Chem.* **1996**, *17*, 49−56.
(52) Hiroshi, N.; Tomoo, M.; Ryoichi, F. Symmetry-Adapted-Cluster/Symmetry-Adapted-Cluster Configuration Interaction Methodology Extended to Giant Molecular Systems: Ring Molecular Crystals. *J. Chem. Phys.* **2007**, *126*, 084104.
(53) Cederbaum, L. S.; Domcke, W. Theoretical Aspects of Ionization Potentials and Photoelectron Spectroscopy: A Green's Function Approach. *Adv. Chem. Phys.* **1977**, *36*, 205−344.
(54) Cederbaum, L. S.; Schirmer, J.; Domcke, W.; von Niessen, W. Complete Breakdown of the Quasiparticle Picture for Inner Valence Electrons. *J. Phys. B* **1977**, *10*, L549−L553.
(55) Raghavachari, K.; Trucks, G. W.; Pople, J. A.; Head-Gordon, M. A Fifth-Order Perturbation Comparison of Electron Correlation Theories. *Chem. Phys. Lett.* **1989**, *157*, 479−483.
(56) Harding, M. E.; Metzroth, T.; Gauss, J.; Auer, A. A. Parallel Calculation of CCSD and CCSD(T) Analytic First and Second Derivatives. *J. Chem. Theory Comput.* **2007**, *4*, 64−74.
(57) Zeng, X.; Yao, L.; Wang, W.; Liu, F.; Sun, Q.; Ge, M.; Sun, Z.; Zhang, J.; Wang, D. Electronic Structures of Acyl Nitrites and Nitrates. *Spectrochim. Acta A* **2006**, *64*, 949−955.
(58) Zeng, X.; Wang, W.; Liu, F.; Ge, M.; Sun, Z.; Wang, D. Electronic Structure of Binary Phosphoric and Arsenic Triazides. *Eur. J. Inorg. Chem.* **2006**, *2006*, 416−421.
(59) Xiaoqing, Z.; Fengyi, L.; Qiao, S.; Maofa, G.; Jianping, Z.; Xicheng, A.; Lingpeng, M.; Shijun, Z.; Dianxun, W. Reaction of AgN_3 with $SOCl_2$: Evidence for the Formation of Thionyl Azide, $SO(N_3)_2$. *Inorg. Chem.* **2004**, *43*, 4799−4801.
(60) Zeng, X.; Bernhardt, E.; Beckers, H.; Willner, H. Synthesis and Characterization of the Phosphorus Triazides $OP(N_3)_3$ and $SP(N_3)_3$. *Inorg. Chem.* **2011**, *50*, 11235−11241.
(61) *CrysAlisPro*, version 1.171.33.42, Oxford Diffraction Ltd.: Abingdon, U.K., 2009.
(62) Farrugia, L. WinGX Suite for Small-Molecule Single-Crystal crystallography. *J. Appl. Crystallogr.* **1999**, *32*, 837−838.
(63) Sheldrick, G. A Short History of SHELX. *Acta Crystallogr.* **2008**, *A64*, 112−122.
(64) Berger, R. J. F.; Hoffmann, M.; Hayes, S. A.; Mitzel, N. W. An Improved Gas Electron Diffractometer - The Instrument, Data Collection, Reduction and Structure Refinement Procedures. *Z. Naturforsch.* **2009**, *64B*, 1259−1268.
(65) Vishnevskiy, Y. V. The Initial Processing of the Gas Electron Diffraction Data: An Improved Method for Obtaining Intensity Curves from Diffraction Patterns. *J. Mol. Struct.* **2007**, *833*, 30−41.
(66) Vishnevskiy, Y. V. The Initial Processing of the Gas Electron Diffraction Data: New Method for Simultaneous Determination of the Sector Function and Electron Wavelength from Gas Standard Data. *J. Mol. Struct.* **2007**, *871*, 24−32.
(67) Sipachev, V. A. Calculation of Shrinkage Corrections in Harmonic Approximation. *J. Mol. Struct. (THEOCHEM)* **1985**, *121*, 143−151.
(68) Sipachev, V. A. The Use of Quantum-Mechanical Third-Order Force Constants in Structural Studies. *J. Mol. Struct.* **2004**, *693*, 235−240.
(69) Sipachev, V. A. Local Centrifugal Distortions Caused by Internal Motions of Molecules. *J. Mol. Struct.* **2001**, *567*−*568*, 67−72.
(70) Vogt, N.; Vishnevskiy, Y. V.; Ivanov, A. A.; Vogt, J.; Vilkov, L. V. *N*-Methylsuccinimide, Molecular Structure from GED and Quantum Chemical Studies. *Russ. J. Phys. Chem. A* **2008**, *82*, 2286−2292.